

# Vortex matter in low dimensional systems with proximity induced superconductivity

N.B. Kopnin,<sup>1,2</sup> I.M. Khaymovich,<sup>3</sup> and A.S. Mel'nikov<sup>3</sup>

<sup>1</sup> *O.V. Lounasmaa Laboratory, Aalto University, P.O. Box 15100, 00076 Aalto, Finland*

<sup>2</sup> *L. D. Landau Institute for Theoretical Physics, 117940 Moscow, Russia*

<sup>3</sup> *Institute for Physics of Microstructures, Russian Academy of Sciences, 603950 Nizhny Novgorod, GSP-105, Russia*

(Dated: March 3, 2018)

We study theoretically the vortex matter structure in low dimensional (LD) systems with superconducting order induced by proximity to a bulk superconductor. We analyze the effects of microscopic coupling mechanisms between the two systems and the effects of possible mismatch in the band structures of these materials on the energy spectrum of vortex-core electrons. The unusual structure of vortex cores is discussed in the context of recent tunneling microscopy/spectroscopy experiments.

PACS numbers: 73.22.-f; 74.45.+c; 74.78.-w

## I. INTRODUCTION.

The induced superconducting order attracts considerable interest of both theorists and experimentalists for many decades starting from the seminal works on the proximity effect.<sup>1,2</sup> Recently, one sees a revival of this interest in connection with the growing number of experiments carried out for a variety of new artificial systems which include two-dimensional electron gas, graphene, semiconducting nanowires and carbon nanotubes, topological insulators, etc. Exotic electronic properties of these systems<sup>3–7</sup> can cause quite unusual manifestations of the proximity effect. Superconducting characteristics of such low-dimensional (LD) systems can differ strongly from those in the bulk. Thus the experiments on proximity induced superconductivity provide a unique possibility to manipulate the basic properties of the superconducting state. Control of superconducting characteristics can be realized by changing the doping level through the gate potential, which creates, e.g., new types of tunable Josephson devices.<sup>8</sup> Unconventional gap potential induces, in turn, unusual quasiparticle (QP) states both in homogeneous and in nonuniform superconducting phases. For LD systems with a nontrivial topological structure one can possibly realize the QP modes with specific symmetries of the electron and hole wave functions at the Fermi level that describe the so-called Majorana fermions in condensed matter.<sup>9,10</sup>

A standard way of studying the QP states in systems with a complicated superconducting order is to look at the effects of applied magnetic field on the structure of the mixed state. For example, if the bulk electrode is a type-II superconductor (SC) one can study the structure of vortex lines penetrating the electrode and threading also the LD system (see Fig. 1). It is the goal of this paper to review the basic properties of the vortex matter formed in the LD layer. Similar problem of the vortex matter in the proximity layers naturally arises when one faces the challenge of interpreting the scanning tunneling microscopy/spectroscopy (STM/STS) measurements in superconductors. Probing the energy and spatial de-

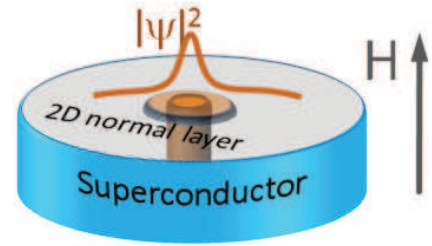


FIG. 1: (Color online) Sketch of the 2D layer with multiple core vortex structure induced by a bulk type II superconductor in the vortex state. Two scales of the induced vortex are schematically depicted by orange disks in 2D layer and cylinder in the bulk superconductor.

pendencies of the local density of states (LDOS) by STM/STS<sup>11</sup> provides information of the spectrum and of the wave functions in the superconducting state. An important part of this information refers to the structure of subgap QP states in the magnetic field bound to the vortex core which are known as the Caroli–de Gennes–Matricon (CdGM) states<sup>12</sup>. A fingerprint of these states is the so-called zero-bias anomaly (ZBA)<sup>11</sup> seen in the STM measurements. Obviously, the intrinsic characteristics of the bound core states can be masked or even hidden by the presence of a thin defect layer at the surface of the bulk SC. In such thin (possibly non-superconducting) surface layer, the superconducting coherence is induced by proximity to the bulk SC. The masking effect of the defect layer is often difficult to distinguish from more exotic explanations based, e.g., on the assumptions of the superconducting gap anisotropy (see<sup>13,14</sup> and references therein) and multi-component structure of the order parameter<sup>15,16</sup>. Despite all its simplicity, the model assuming the presence of a defect layer at the sample surface can explain quite a variety of features in the vortex LDOS experimental data and provides an instructive example of the vortex matter in the LD systems with the induced superconducting order.

Instead of considering various phenomenological mod-

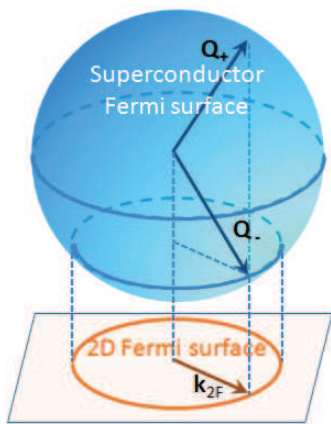


FIG. 2: (Color online) Matching of Fermi surfaces in 2D layer and in the bulk superconductor in the coherent tunneling case. In the simple case of isotropic Fermi surfaces the in-plane projections of 3D Fermi momenta  $\mathbf{Q}_{\pm}$  coincide with the Fermi momentum in 2D layer  $\mathbf{k}_{2F}$ .

els of the induced gap potential, in our studies of the vortex matter we rather use the general microscopic approach developed in Ref. 17 and focus on the physical mechanisms responsible for formation of the particular gap potential and its symmetry. These mechanisms are mostly determined by the nature of the electron transfer between the two-dimensional (2D) proximity system and the bulk SC. This transfer is strongly affected by both the mismatch of the band structures in the coupled subsystems and by disorder in the barrier between them. Without disorder and neglecting the band structure effects one arrives at the coherent tunneling model according to which the in-plane projection of the electron momentum is conserved in course of tunneling. The induced gap potential is determined by matching of the 2D Fermi surface with the in-plane projection of the 3D Fermi surface (see Fig. 2). A generalization of the above model can include umklapp processes accounting for the Bloch – type single-electron wave functions in both subsystems. In the latter case, the momentum of tunneling electrons is conserved only up to certain vectors of the reciprocal lattices. One more limiting case is the so-called incoherent tunneling model which assumes a strong disorder in the tunneling barrier and allows for an arbitrary random change in the momenta of tunneling electrons. The systematic analysis of these three tunneling models shows that the gap potential strongly depends on the degree of disorder as well as on the band structure effects.

Based on these models we consider several fundamental properties of the vortex matter in the systems with induced superconducting order. First, the proximity induced superconducting gap  $\Delta_{2D}$  is responsible for appearance of a new length scale in the vortex structure, the 2D coherence length,  $\xi_{2D} = \hbar v_{2F}/\Delta_{2D}$  or  $\xi_{2D} = \sqrt{\hbar D_{2D}/\Delta_{2D}}$  for clean or dirty limits, respectively. Here  $v_{2F}$  and  $D_{2D}$  are the Fermi velocity and diffusion constant in the 2D layer. The energy gap  $\Delta_{2D}$  depends

on the tunneling rate  $\Gamma^{17-20}$ ; for example,  $\Delta_{2D} \approx \Gamma$  for  $\Gamma \ll \Delta$ . Since  $\Delta_{2D} \ll \Delta$  the coherence length  $\xi_{2D}$  usually is much longer than the coherence length in the bulk SC,  $\xi_S = \hbar v_F/\Delta$  for clean or  $\xi_S = \sqrt{\hbar D_S/\Delta}$  for dirty limit, where  $\Delta$ ,  $v_F$  and  $D_S$  are the gap, the Fermi velocity and diffusion constant in the superconducting electrode. As a result, all the effects associated with overlapping of neighboring vortex cores as well as the normal QP scattering at the boundary of the 2D system become much more pronounced than in the primary superconducting electrode. There appears, e.g., an intriguing possibility to get a new type of vortex matter strongly bonded by the intervortex QP tunneling even for magnetic fields well below the upper critical field of the bulk superconductor.

Second, hybridization of the localized QP states inside much larger induced vortex cores with the core states of primary vortices in the bulk electrode leads to peculiar structure of the subgap energy branches. For coherent tunneling, the electronic spectrum of a singly quantized vortex consists of two anomalous branches crossing zero of energy as functions of the impact parameter  $b$ . One branch,  $\epsilon_1(b)$ , qualitatively follows the usual CdGM spectrum  $\epsilon_0(b)$  of the primary vortex; it extends above the induced gap where it turns into a scattering resonance. The other branch,  $\epsilon_2(b)$ , lies below the induced gap and resembles the CdGM spectrum for a vortex with a much larger core radius  $\sim \xi_{2D}$ . Thus, the proximity induced vortex in a ballistic 2D layer has a “multiple core” structure characterized by the two length scales,  $\xi_S$  and  $\xi_{2D}$ . Such a two-scale feature does not appear if the proximity vortex states are induced by a primary vortex pinned at a large-size hollow cylinder  $r_0 > \xi_S$ , see Refs.<sup>21,22</sup>.

The spatial and energy dependence of the LDOS inside the multiple core reveals a rich behavior which depends on many parameters and on the degree of disorder both inside the bulk electrode and inside the 2D layer, as well as by the barrier disorder. The barrier disorder suppresses the influence of the primary CdGM spectral branch and leads to broadening of the lower anomalous branch  $\epsilon_2(b)$  due to the momentum uncertainty. Impurity scattering in the bulk and/or inside the 2D layer causes further smearing of the spectral characteristics of the core states which then approach the usual dirty-SC LDOS scaled with the corresponding coherence lengths  $\xi_{2D}$ .

And finally, both the nontrivial topological properties of the normal state wave functions and the induced pairing symmetry can affect the presence of the zero energy states in the QP spectrum of vortices. This phenomenon arises from the wave function symmetry under precession of the subgap QP trajectories inside the vortex core through the corresponding change in the Bohr – Sommerfeld quantization rule for the angular momentum.

The paper is organized as follows. In section II we introduce the basic model used further for the analysis of the induced superconductivity. The derivation of self energies of 2D quasiclassical Eilenberger equations in a

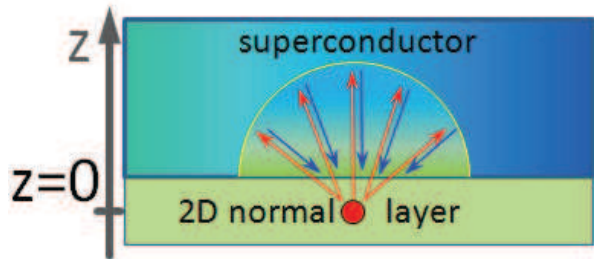


FIG. 3: (Color online) 2D normal metallic layer ( $Z = 0$ ) coupled to a bulk superconducting half-space  $Z > 0$  through a tunneling barrier. The electron waves depicted by red arrows tunnel from the source placed in 2D layer (red solid circle). If the energy is smaller than the superconducting gap, they do not penetrate deep into the bulk superconductor but undergo Andreev reflection to the hole waves (blue arrows) and return to the 2D layer.

vortex state of the bulk superconductor is given in section III. In section IV we discuss the method used for the calculation of the subgap state structure in the induced vortex core. The main results are presented in sections V and VI. In particular, section V contains the results for the subgap spectrum and the local density of states in a induced vortex state of 2D layer. In section VII we discuss implications of our analysis for induced vortex core states in graphene. We also discuss some further implications of a large value of the induced coherence length  $\xi_{2D}$  for the spectral and spatial characteristics of various vortex configurations. Some details of our calculations are given in Appendix.

## II. MODEL.

Consider a 2D normal metallic layer ( $Z = 0$ ) placed in a tunneling contact with a bulk superconducting half-space  $Z > 0$  with a thin insulating barrier between them, see Fig. 3. The Hamiltonian of our system has the form  $\hat{H} = \hat{H}_S + \hat{H}_{2D} + \hat{H}_T$ , where

$$\hat{H}_S = \int d^3R \left[ \sum_{\sigma} \hat{\Psi}_{\sigma}^{\dagger}(\mathbf{X}) (\hat{\epsilon}_{3D} - E_F) \hat{\Psi}_{\sigma}(\mathbf{X}) + \Delta(\mathbf{R}) \hat{\Psi}_{\uparrow}^{\dagger}(\mathbf{X}) \hat{\Psi}_{\downarrow}^{\dagger}(\mathbf{X}) + \Delta^*(\mathbf{R}) \hat{\Psi}_{\downarrow}(\mathbf{X}) \hat{\Psi}_{\uparrow}(\mathbf{X}) \right] \quad (1)$$

is the part describing the superconductor with the  $s$ -wave order parameter  $\Delta(\mathbf{R})$ ,  $\hat{\epsilon}_{3D}$  is the kinetic energy operator, and

$$\hat{H}_{2D} = d \int d^2r \sum_{\sigma} \hat{a}_{\sigma}^{\dagger}(\mathbf{x}) [\hat{\epsilon}_{2D} - E_F] \hat{a}_{\sigma}(\mathbf{x}) \quad (2)$$

is the 2D layer Hamiltonian. We introduce space-time variables  $\mathbf{X} = (\mathbf{R}, \tau)$  and  $\mathbf{x} = (\mathbf{r}, \tau)$  where  $\mathbf{R}$  is a three-dimensional vector in the bulk superconducting region

while  $\mathbf{r}$  is a two-dimensional vector in the normal layer, respectively;  $\tau$  is an imaginary time variable in the standard Matsubara technique. The chemical potential  $E_F$  is supposed to be equal in the subsystems. The single-particle Hamiltonian in the 2D layer  $\hat{\epsilon}_{2D}$  includes the kinetic energy and, in general, the lattice potential corresponding to the crystal structure of the normal system. For simplicity we neglect the band structure of the bulk superconductor. This approximation should be valid for a wide class of heterostructures where the Fermi surface in the bulk SC is large compared with that in the 2D layer. We assume that tunneling is spin-independent and occurs locally in time and in space, i.e., from the point near the interface  $\mathbf{R} = (\mathbf{r}, Z = 0)$  on the superconductor side into the point  $\mathbf{r}$  in the layer and back with the amplitude  $t(\mathbf{r})$  that depends on the coordinate of the tunneling center on the interface. Since the tunneling amplitude accounts for certain region of an atomic size in the vicinity of tunneling center, the wave function magnitude at  $Z = 0$  should be considered as an average value near the exact boundary of the superconducting region. The tunneling amplitude is assumed small in the atomic scale. More detailed restrictions for the value of tunneling amplitude will be considered later. The tunneling Hamiltonian has the form

$$\hat{H}_T = d \sum_{\sigma} \int \left[ t(\mathbf{r}) \hat{\Psi}_{\sigma}^{\dagger}(\mathbf{x}) a_{\sigma}(\mathbf{x}) + t^*(\mathbf{r}) \hat{a}_{\sigma}^{\dagger}(\mathbf{x}) \hat{\Psi}_{\sigma}(\mathbf{x}) \right] d^2r \quad (3)$$

where the wave functions in the superconductor are taken at the space-time point  $\mathbf{x}$  at the interface  $Z = 0$ .

The Matsubara Green functions take the form:

$$\langle T_{\tau} \hat{a}_{\alpha}(\mathbf{x}_1) \hat{a}_{\beta}^{\dagger}(\mathbf{x}_2) \rangle = \delta_{\alpha\beta} G(\mathbf{x}_1, \mathbf{x}_2), \quad (4a)$$

$$\langle T_{\tau} \hat{\Psi}_{\alpha}(\mathbf{X}_1) \hat{a}_{\beta}^{\dagger}(\mathbf{x}_2) \rangle = \delta_{\alpha\beta} G_T(\mathbf{X}_1, \mathbf{x}_2), \quad (4b)$$

$$\langle T_{\tau} \hat{\Psi}_{\alpha}(\mathbf{X}_1) \hat{\Psi}_{\beta}^{\dagger}(\mathbf{X}_2) \rangle = \delta_{\alpha\beta} G_S(\mathbf{X}_1, \mathbf{X}_2), \quad (4c)$$

and

$$\langle T_{\tau} \hat{a}_{\alpha}(\mathbf{x}_1) \hat{a}_{\beta}(\mathbf{x}_2) \rangle = i \hat{\sigma}_{\alpha\beta}^{(y)} F(\mathbf{x}_1, \mathbf{x}_2), \quad (5a)$$

$$\langle T_{\tau} \Psi_{\alpha}(\mathbf{X}_1) \hat{a}_{\beta}(\mathbf{x}_2) \rangle = i \hat{\sigma}_{\alpha\beta}^{(y)} F_T(\mathbf{X}_1, \mathbf{x}_2), \quad (5b)$$

$$\langle T_{\tau} \hat{\Psi}_{\alpha}(\mathbf{X}_1) \hat{\Psi}_{\beta}(\mathbf{X}_2) \rangle = i \hat{\sigma}_{\alpha\beta}^{(y)} F_S(\mathbf{X}_1, \mathbf{X}_2), \quad (5c)$$

etc. Equations for the Green functions can be more conveniently written in the frequency representation  $\omega_n = (2n + 1)\pi T$ . We denote  $\tau = \tau_1 - \tau_2$  and write

$$G(\mathbf{r}_1, \mathbf{r}_2) = \int_0^{\hbar/T} G(\mathbf{r}_1, \mathbf{r}_2; \tau) e^{i\omega_n \tau / \hbar} d\tau,$$

skipping for simplicity the subscript. We introduce also the Nambu matrices for Hamiltonian and Green functions

$$\check{H}_S = \begin{pmatrix} \hat{\epsilon}_{3D} - E_F & -\Delta(\mathbf{R}) \\ \Delta^*(\mathbf{R}) & \hat{\epsilon}_{3D} - E_F \end{pmatrix}, \quad \check{G} = \begin{pmatrix} G & F \\ -F^{\dagger} & \check{G} \end{pmatrix},$$

and denote the inverse operators

$$\begin{aligned}\check{G}_S^{-1}(\mathbf{R}) &= -i\check{\tau}_3\omega_n + \check{H}_S, \\ \check{G}_{2D}^{-1}(\mathbf{r}) &= -i\check{\tau}_3\omega_n + \check{\tau}_0 \otimes [\hat{\epsilon}_{2D} - E_F],\end{aligned}$$

in the superconductor and 2D layer, respectively.

Equations for the mixed Green functions  $\check{G}_T(\mathbf{R}_1, \mathbf{r}_2)$  can be written in the form

$$\check{G}_S^{-1}(\mathbf{R}_1)\check{G}_T(\mathbf{R}_1, \mathbf{r}_2) + d\check{t}(\mathbf{R}_{1\perp})\check{G}(\mathbf{R}_{1\perp}, \mathbf{r}_2)\delta(Z_1) = 0$$

where  $Z_1 \geq 0$ ,  $\mathbf{R}_1 = (\mathbf{R}_{1\perp}, Z_1)$  and

$$\check{t}(\mathbf{r}) = \begin{pmatrix} t(\mathbf{r}) & 0 \\ 0 & t^*(\mathbf{r}) \end{pmatrix}.$$

Neglecting the back-action of a thin 2D layer on the superconductor, we assume that the superconducting Green function  $\check{G}_S(\mathbf{R}_1, \mathbf{R}_2)$  is a non-interacting function that satisfies

$$\check{G}_S^{-1}(\mathbf{R}_1)\check{G}_S(\mathbf{R}_1, \mathbf{R}_2) = \check{1}\hbar\delta(\mathbf{R}_1 - \mathbf{R}_2) \quad (6)$$

in the range  $Z_{1,2} > 0$ . The boundary conditions for  $\check{G}_S(\mathbf{R}_1, \mathbf{R}_2)$  at  $Z = 0$  depend on the particular interface in the absence of tunneling. This gives

$$\check{G}_T(\mathbf{R}_1, \mathbf{r}_2) = -\frac{d}{\hbar} \int \check{G}_S(\mathbf{R}_1, \mathbf{r}')\check{t}(\mathbf{r}')\check{G}(\mathbf{r}', \mathbf{r}_2) d^2r' \quad (7)$$

Equations for the Green functions in the layer can be written as

$$\begin{aligned}\check{G}_{2D}^{-1}(\mathbf{r}_1)\check{G}(\mathbf{r}_1, \mathbf{r}_2) + \check{t}^*(\mathbf{r}_1)\check{G}_T(\mathbf{r}_1, \mathbf{r}_2) \\ = \check{1}d^{-1}\hbar\delta(\mathbf{r}_1 - \mathbf{r}_2)\end{aligned}$$

Using Eq. (7) we find

$$\begin{aligned}\check{G}_{2D}^{-1}(\mathbf{r}_1)\check{G}(\mathbf{r}_1, \mathbf{r}_2) - \int \check{\Sigma}_T(\mathbf{r}_1, \mathbf{r}')\check{G}(\mathbf{r}', \mathbf{r}_2) d^2r' \\ = \check{1}\hbar d^{-1}\delta(\mathbf{r}_1 - \mathbf{r}_2), \quad (8)\end{aligned}$$

where

$$\check{\Sigma}_T(\mathbf{r}_1, \mathbf{r}') = \begin{pmatrix} \Sigma_1 & \Sigma_2 \\ -\Sigma_2^\dagger & \bar{\Sigma}_1 \end{pmatrix} = \frac{d}{\hbar}\check{t}^*(\mathbf{r}_1)\check{G}_S^0(\mathbf{r}_1, \mathbf{r}')\check{t}(\mathbf{r}'). \quad (9)$$

One can introduce the momentum representation of the Green function<sup>23</sup>

$$\check{G}_S(\mathbf{R}_1, \mathbf{R}_2) = \int \frac{d^3Q_1}{(2\pi)^3} \frac{d^3Q_2}{(2\pi)^3} \check{G}_S(\mathbf{Q}_1, \mathbf{Q}_2) e^{i\mathbf{Q}_1\mathbf{R}_1 - i\mathbf{Q}_2\mathbf{R}_2}. \quad (10)$$

and the tunneling coefficients:  $\check{t}(\mathbf{r}) = \int \frac{d^2q}{(2\pi)^2} \check{t}(\mathbf{q}) e^{i\mathbf{q}\mathbf{r}}$ . The Fourier representation for the Green functions in the 2D layer is

$$\check{G}(\mathbf{r}_1, \mathbf{r}_2) = \int \frac{d^2q_1}{(2\pi)^2} \frac{d^2q_2}{(2\pi)^2} \check{G}(\mathbf{q}_1, \mathbf{q}_2) e^{i\mathbf{q}_1\mathbf{r}_1 - i\mathbf{q}_2\mathbf{r}_2}. \quad (11)$$

## A. Tunneling with umklapp processes.

The crystal structure of the 2D layer accounts for an atomic-scale periodic potential in Eq. (8) which mixes the Fourier harmonics with the momenta shifted by the reciprocal lattice vectors  $\mathbf{b}$ . Using the Bloch functions

$$\psi_m(\mathbf{k}, \mathbf{r}) = \sum_{\mathbf{b}} e^{i(\mathbf{k}+\mathbf{b})\mathbf{r}} u_{m\mathbf{k}+\mathbf{b}}$$

diagonalizing the single-particle energy operator inside the layer

$$\epsilon_{2D}(\mathbf{r})\psi_m(\mathbf{k}, \mathbf{r}) = \epsilon_m(k)\psi_m(\mathbf{k}, \mathbf{r})$$

one can conveniently introduce the field operators  $\hat{a}_{\alpha,m,\mathbf{k}}$

$$\hat{a}_\alpha(\mathbf{r}) = \sum_m \int \frac{d^2k}{(2\pi)^2} \hat{a}_{\alpha,m,\mathbf{k}} \psi_m(\mathbf{k}, \mathbf{r}).$$

The index  $m$  enumerates the energy bands.

Introducing the corresponding Green functions

$$\langle T_\tau \hat{a}_{\alpha,m_1,\mathbf{k}_1} \hat{a}_{\beta,m_2,\mathbf{k}_2}^\dagger \rangle = \delta_{\alpha\beta} G_{m_1,m_2}(\mathbf{k}_1, \mathbf{k}_2), \quad (12a)$$

$$\langle T_\tau \hat{a}_{\alpha,m_1,\mathbf{k}_1} \hat{a}_{\beta,m_2,-\mathbf{k}_2} \rangle = i\hat{\sigma}_{\alpha\beta}^{(y)} F_{m_1,m_2}(\mathbf{k}_1, \mathbf{k}_2), \quad (12b)$$

one can diagonalize the operator  $\check{G}_{2D}^{-1}$  in Eq. (8) in the Bloch representation,

$$\check{G}_{2D,m}^{-1}(\mathbf{k}) = -i\hbar\check{\tau}_3\omega_n + \begin{pmatrix} \epsilon_m(\mathbf{k}) - E_F & 0 \\ 0 & \epsilon_m(-\mathbf{k}) - E_F \end{pmatrix}. \quad (13)$$

We assume in what follows that the amplitude  $\Delta_{ind}$  of the induced superconducting gap  $\Delta_{2D}$  is small compared to the interband distance  $\epsilon_m - \epsilon_{m'}$  and neglect the interband scattering. Hereafter we omit the subscripts  $m$ . At the same time, the transformation from the momentum to the quasimomentum representation results in the mixing of Fourier harmonics in the self energy in Eq. (8). Finally, Eq. (8) for the Green functions (12) takes the form:

$$\begin{aligned}\check{G}_{2D}^{-1}(\mathbf{k}_1)\check{G}(\mathbf{k}_1, \mathbf{k}_2) - \int \check{\Sigma}_T(\mathbf{k}_1, \mathbf{k}')\check{G}(\mathbf{k}', \mathbf{k}_2) d^2k' \\ = \hbar\check{1}\delta(\mathbf{k}_1 - \mathbf{k}_2), \quad (14)\end{aligned}$$

with

$$\check{\Sigma}_T(\mathbf{k}_1, \mathbf{k}') = \frac{d}{\hbar} \int \check{t}_b^+(\mathbf{k}_1, \mathbf{Q}_\perp) \check{G}_S^0(\mathbf{Q}, \mathbf{Q}') \check{t}_b(\mathbf{Q}_\perp, \mathbf{k}') d^3Q d^3Q',$$

$$\check{t}_b(\mathbf{Q}, \mathbf{k}) = \sum_{\mathbf{b}} u_{\mathbf{k}+\mathbf{b}} \check{t}(\mathbf{Q}_\perp - \mathbf{k} - \mathbf{b}) \quad (15)$$

and  $\check{t}_b^+(\mathbf{k}, \mathbf{Q}_\perp) = \check{t}_b^*(\mathbf{Q}_\perp, \mathbf{k})$ . Here  $\mathbf{Q} = (\mathbf{Q}_\perp, Q_z)$ . The above expression for the tunneling coefficients  $t_b$  describes in fact the umklapp processes caused by the periodic crystal potential in the 2D layer.

## B. Coherent tunneling

The simplest model of tunneling assumes that the in-plane momentum projection of electrons is conserved during the tunneling process:  $\check{t}(\mathbf{Q}_\perp - \mathbf{k}) = \check{t} \cdot \delta(\mathbf{Q}_\perp - \mathbf{k})$ . This is equivalent to the assumption that the tunneling amplitude  $t(\mathbf{r})$  is independent of the coordinate along the SC/2D interface. Of course, the quasimomentum conservation is not exact in the presence of energy bands since the tunneling mixes the quasimomentum values which differ by a reciprocal lattice vector:  $\check{t}_b(\mathbf{Q}, \mathbf{k}) = \check{t} \sum_{\mathbf{b}} u_{\mathbf{k}+\mathbf{b}} \delta(\mathbf{Q}_\perp - \mathbf{k} - \mathbf{b})$ . Neglecting umklapp processes for simplicity we find from Eq. (14)

$$\check{\Sigma}_T(\mathbf{k}_1, \mathbf{k}') = \frac{dt^2}{\hbar} \int \check{G}_S^0(\mathbf{k}_1, Q_z; \mathbf{k}', Q'_z) \frac{dQ_z dQ'_z}{(2\pi)^2}.$$

From now on we will use the quasiclassical approximation for the Green functions. In order to derive the Eilenberger equations in the 2D layer we follow the standard procedure described, e.g., in Ref. 23. First of all we introduce the average  $\mathbf{k} = (\mathbf{k}_1 + \mathbf{k}_2)/2$ ,  $Q_z = (Q_{1z} + Q_{2z})/2$  and relative  $\mathbf{k}_- = \mathbf{k}_1 - \mathbf{k}_2$ ,  $q_z = Q_{1z} - Q_{2z}$  momenta and denote  $\check{G}(\mathbf{k}_1, \mathbf{k}_2) = \check{G}(\mathbf{k}, \mathbf{k}_-)$ ,  $\check{G}_S(\mathbf{k}_1, Q_{1z}; \mathbf{k}_2, Q_{2z}) = \check{G}_S(\mathbf{k}, Q_z; \mathbf{k}_-, q_z)$ . Next we apply the operator  $\check{G}_{2D}^{-1}$  to the Green function  $\check{G}(\mathbf{k}, \mathbf{k}_-)$  from the right and subtract this equation from Eq. (14). We now transform to the quasiclassical Green functions by integrating the resulting equation over  $d\xi_2$  where  $\xi_2 = \epsilon_{2D}(\mathbf{k}) - E_F$ . The Green functions are to be taken in the vicinity of the Fermi surface. Therefore, in the mixed momentum-coordinate representation,

$$\begin{aligned} \check{G}(\mathbf{k}, \mathbf{r}) &= \int \check{G}(\mathbf{k}, \mathbf{k}_-) e^{i\mathbf{k} \cdot \mathbf{r}} \frac{d^2 k_-}{(2\pi)^2} \\ \check{G}_S(\mathbf{k}, Q_z; \mathbf{r}, Z) &= \int \check{G}_S(\mathbf{k}, Q_z; \mathbf{k}_-, q_z) e^{i\mathbf{k} \cdot \mathbf{r} + iq_z Z} \frac{d^2 k_- dQ_z}{(2\pi)^3} \end{aligned}$$

we can put

$$\begin{aligned} \check{G}_S(\mathbf{k}, Q_z; \mathbf{r}, Z) &= \check{g}_S(\mathbf{k}, Q_z; \mathbf{r}, Z) \pi i \delta_\Delta(\xi_3), \\ \check{G}(\mathbf{k}, \mathbf{r}) &= \check{g}(\mathbf{k}, \mathbf{r}) \pi i \delta_\Delta(\xi_2) \end{aligned}$$

Here the standard quasiclassical Green functions are

$$\check{g}(\mathbf{k}_{2F}, \mathbf{r}) = \frac{1}{\pi i} \int d\xi_2 \check{G}(\mathbf{k}, \mathbf{r}), \quad (16)$$

$$\check{g}_S(\mathbf{K}_F, \mathbf{R}) = \frac{1}{\pi i} \int d\xi_3 \check{G}_S(\mathbf{Q}, \mathbf{R}). \quad (17)$$

$\xi_3 = \epsilon_S(\mathbf{Q}) - E_F$  is the normal QP spectrum in the 3D half-space, and  $\delta_\Delta(\xi_{2,3})$  is a delta function broadened at the gap energy scale  $\Delta$ .

At the next step of derivation we note that, in the mixed representation, the term

$$\int \frac{d\xi_2}{\pi i} \int \check{\Sigma}_T(\mathbf{k}_1, \mathbf{k}') \check{G}(\mathbf{k}', \mathbf{k}_2) \frac{d^2 k'}{(2\pi)^2}$$

in the equation for the Green function becomes

$$\begin{aligned} &\frac{\pi i dt^2}{\hbar} \int d\xi_2 \int \frac{dQ_z}{2\pi} \check{g}_S(\mathbf{k}, Q_z; \mathbf{r}, 0) \check{g}(\mathbf{k}, \mathbf{r}) \delta_\Delta(\xi_3) \delta_\Delta(\xi_2) \\ &= \frac{\pi i dt^2}{\hbar} \int \frac{dQ_z}{2\pi} \check{g}_S(\mathbf{Q}; \mathbf{r}, 0) \check{g}(\mathbf{k}_{2F}, \mathbf{r}) \times \delta_\Delta[\epsilon_{3D}(\mathbf{Q}) - E_F] \end{aligned}$$

where  $\mathbf{Q} = (\mathbf{k}_{2F}, Q_z)$  has the in-plane projection coinciding with the 2D Fermi momentum  $\mathbf{k}_{2F}$ .

Finally, we obtain the quasiclassical Eilenberger equation for retarded (advanced) Green functions

$$\begin{aligned} &-i\hbar \mathbf{v}_{2F} \nabla \check{g}(\mathbf{k}_{2F}, \mathbf{r}) - \epsilon [\check{r}_3 \check{g}(\mathbf{k}_{2F}, \mathbf{r}) - \check{g}(\mathbf{k}_{2F}, \mathbf{r}) \check{r}_3] \\ &- [\check{\Sigma}_T \check{g}(\mathbf{k}_{2F}, \mathbf{r}) - \check{g}(\mathbf{k}_{2F}, \mathbf{r}) \check{\Sigma}_T] = 0, \quad (18) \end{aligned}$$

where  $\hbar \mathbf{v}_{2F} = \partial \epsilon_{2D}(\mathbf{k}) / \partial \mathbf{k}$  is the 2D layer Fermi velocity.

For isotropic Fermi surfaces in both the superconductor  $\epsilon_{3D}(\mathbf{Q}) = \hbar^2 Q^2 / 2m$  and the 2D layer  $\epsilon_m(\mathbf{k}) = \hbar^2 k^2 / 2m_{2D}$ , the self energy takes the form

$$\check{\Sigma}_T(\mathbf{k}_{2F}, \mathbf{r}) = \frac{i\Gamma}{2} [\check{g}_S(\mathbf{Q}_+; \mathbf{r}, 0) + \check{g}_S(\mathbf{Q}_-; \mathbf{r}, 0)], \quad (19)$$

with the tunneling rate

$$\Gamma = dt^2 \int_0^\infty \delta_\Delta[\epsilon_S(\mathbf{k}_{2F}, Q_z) - E_F] dQ_z.$$

The 3D momentum  $\mathbf{Q}_\pm = (\mathbf{k}_{2F}, \pm Q_{3z})$  lies on the Fermi surface of the bulk SC,  $k_{2F}^2 + Q_{3z}^2 = K_F^2$ . Provided the 2D Fermi surface is smaller than the extremal cross section of the 3D Fermi surface, i.e.,  $k_{2F} < K_F$  the expression for the tunneling rate reads:  $\Gamma = dmt^2 / Q_{3z}$ . For large 2D Fermi surfaces  $k_{2F} > K_F$  the self-energy term vanishes, and the coherent tunneling is impossible. The case of momenta  $k_{2F} \simeq K_F$  deserves special consideration which should take account of a finite delta function width:  $\Gamma \sim dt^2(m/\Delta)^{1/2}$ .

The umklapp processes should, of course, modify the self-energy part resulting in additional contributions:

$$\check{\Sigma}_T(\mathbf{k}_{2F}, \mathbf{r}) = \sum_{\mathbf{b}} |u_{\mathbf{k}_{2F}+\mathbf{b}}|^2 \check{\Sigma}_T^{(0)}(\mathbf{k}_{2F} + \mathbf{b}, \mathbf{r}), \quad (20)$$

where  $\check{\Sigma}_T^{(0)}(\mathbf{k}_{2F}, \mathbf{r})$  is given by the Eq.(19).

## C. Incoherent tunneling

The coherent tunneling model in many cases oversimplifies the realistic experimental situation. The momentum conservation is violated, for example, by the presence of disorder at the interface. Here we consider an opposite limit of strong disorder, which is sometimes called the incoherent tunneling model. This model assumes a random tunneling process of electrons through the barrier in a way similar to the standard theory of dirty metals

within the Born approximation<sup>24</sup>. We assume that the ensemble average of tunneling amplitudes is

$$\overline{t(\mathbf{r}_1)t(\mathbf{r}_2)} = t^2 s_a \delta(\mathbf{r}_1 - \mathbf{r}_2), \quad (21)$$

where  $s_a$  is the correlated area of the order of atomic scale. Following the standard diagrammatic procedure we expand the solution for the ensemble averaged Green function in a series in the scattering field and split the multiple correlators of the  $t(\mathbf{r})$  values in a product of the above pair correlators. Finally, after averaging the self energy (9) becomes:

$$\begin{aligned} \check{\Sigma}_T(\mathbf{r}_1, \mathbf{r}_2) &= t^2 ds_a \check{G}_S(\mathbf{r}_1, \mathbf{r}_1; 0) \delta(\mathbf{r}_1 - \mathbf{r}_2) \\ &= t^2 ds_a i\pi\nu_3(0) \langle \check{g}_S(\mathbf{Q}; \mathbf{r}, 0) \rangle \delta(\mathbf{r}_1 - \mathbf{r}_2). \end{aligned} \quad (22)$$

Here  $\nu_3(0)$  is the normal density of states in the bulk material. Angular brackets denote averaging over three-dimensional momentum directions. Within the quasiclassical approach, the resulting self energy to be used in the Eilenberger equation (18) is given by

$$\check{\Sigma}_T(\mathbf{r}) = i\Gamma \langle \check{g}_S(\mathbf{Q}; \mathbf{r}, 0) \rangle. \quad (23)$$

where the tunneling rate is  $\Gamma = \pi\nu_3(0)ds_a t^2$ . This approximation coincides with that used in Ref. 17. The tunneling rate  $\Gamma \sim t^2/E_F$  can be expressed<sup>17</sup> in terms of the normal-state tunnel conductance  $G = 1/RS$  per unit contact area,  $\Gamma = G/(4\pi G_0\nu_2) \sim E_F R_0/R$ , with the conductance quantum  $G_0 = e^2/\pi\hbar$  and the normal 2D density of states (DOS)  $\nu_2 = m_{2D}/2\pi\hbar^2$ . Therefore  $\Gamma/E_F \ll 1$  if the total tunnel resistance  $R$  is much larger than the Sharvin resistance  $R_0 = (NG_0)^{-1}$  for an ideal  $N$ -mode contact with the contact area  $S$ . Nevertheless, there is a room for the condition  $\Gamma \sim \Delta$  to be fulfilled even for the large contact resistance  $R \gg R_0$ .

#### D. Adiabatic approximation. Range of validity.

The above microscopic analysis allows us to comment on the simplest phenomenological model which is often used for description of the proximity induced superconductivity, see for example,<sup>22,25-27</sup>. Within this model, the Bogoliubov – de Gennes equations inside the proximity superconductor include a phenomenological gap function which is postulated to be proportional to the gap function  $\Delta$  inside the superconducting electrode. Our approach shows that this is generally not the case. The true equation (18) includes self-energies which are complicated functions of energy, coordinates, and momentum. In fact, the effective gap function resembles that in a usual superconductor only if the bulk SC is homogeneous in space. In this case, the quasiclassical Green function is

$$\check{g}_\epsilon^{R(A)} = \pm \frac{1}{\sqrt{\epsilon^2 - |\Delta|^2}} \begin{pmatrix} \epsilon & \Delta \\ -\Delta^* & -\epsilon \end{pmatrix}$$

In this case the self energy is  $\check{\Sigma}_T = i\Gamma\check{g}_S$ , for both coherent and incoherent tunneling models. This expression also holds if the superconducting gap is a slow function of coordinates on distances of the order of  $\xi_S$ . For  $|\epsilon| < |\Delta|$  the self-energy has the form

$$\check{\Sigma}_T(\mathbf{r}) = \frac{\Gamma}{\sqrt{|\Delta(\mathbf{r})|^2 - \epsilon^2}} \begin{pmatrix} \epsilon & \Delta(\mathbf{r}) \\ -\Delta^*(\mathbf{r}) & -\epsilon \end{pmatrix}. \quad (24)$$

Only for low-transparency tunnel contact,  $\Gamma \ll \Delta$ , this self energy is nearly off-diagonal on the scale  $\epsilon \sim \Gamma$  and can be regarded as an energy-independent effective gap function

$$\check{\Sigma}_T \simeq i\Gamma\check{\tau}_2 e^{i\tilde{\tau}_3\phi}, \quad (25)$$

where  $\phi$  is the phase of the superconducting order parameter. Note that the resulting induced gap does not at all depend on the gap magnitude  $|\Delta|$  in the bulk. If the transparency is finite, the electronic spectrum in the induced superconductor has a gap  $\Delta_{2D}$  which is determined by the condition<sup>1,17</sup>

$$(\epsilon + \Sigma_1)^2 - \Sigma_2^2 = 0, \quad \epsilon = \Delta_{2D}. \quad (26)$$

Of course, the adiabatic approximation also breaks down if the order parameter  $\Delta$  varies as a function of coordinates at distances of the order of coherence length in the superconducting electrode, when the self-energies are no longer determined by Eq. (24).

### III. VORTEX POTENTIALS AND GREEN FUNCTIONS FOR CLEAN SYSTEMS

The quasiclassical Green functions in the 2D layer satisfy the Eilenberger equations (18). In components,

$$-i\hbar\mathbf{v}_{2F}\nabla f - 2(\epsilon + \Sigma_1)f + 2\Sigma_2g = 0, \quad (27a)$$

$$i\hbar\mathbf{v}_{2F}\nabla f^\dagger - 2(\epsilon + \Sigma_1)f^\dagger + 2\Sigma_2^\dagger g = 0, \quad (27b)$$

$$-i\hbar\mathbf{v}_{2F}\nabla g + \Sigma_2 f^\dagger - \Sigma_2^\dagger f = 0. \quad (27c)$$

and the normalization condition  $g^2 - ff^\dagger = 1$  with the self energies Eqs. (19) or (23) as effective potentials.

In this and the following Section we consider the case of isotropic Fermi surfaces. Modifications due to the anisotropy of the spectrum are discussed in Section V B. QPs in clean systems are conveniently described by the coordinates along their trajectories (see Fig. 4). A quasiclassical trajectory is parameterized by its angle  $\alpha$  with the  $x$  axis, the impact parameter  $b = \rho \sin(\phi - \alpha)$  and the coordinate  $s = \rho \cos(\phi - \alpha)$  along the trajectory. We introduce the symmetric and antisymmetric parts of the Green functions as it was done in<sup>23,28</sup>:

$$f = -[\zeta(s) + i\theta(s)] \exp(i\alpha) \quad (28a)$$

$$f^\dagger = [\zeta(s) - i\theta(s)] \exp(-i\alpha), \quad (28b)$$

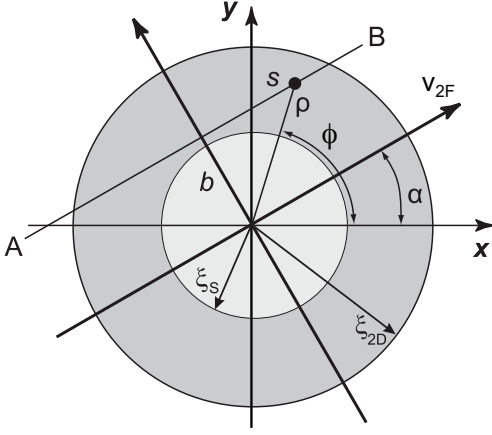


FIG. 4: (Color online) The coordinate frame near the multiple vortex core. Primary (induced) core is shown by the white (gray) circle. The QP trajectory with an impact parameter  $b$  (line AB) passes through the point  $(\rho, \phi)$  shown by the black dot.

where  $\zeta(s) = \zeta(-s)$ , and  $\theta(s) = -\theta(-s)$ . The normalization condition requires  $g^2 + \theta^2 + \zeta^2 = 1$ . Eilenberger equations (27) can be rewritten in the form

$$\hbar v_{2F} \frac{d\zeta}{ds} + 2(\epsilon + \Sigma_1)\theta - 2ig\Sigma_R = 0, \quad (29a)$$

$$\hbar v_{2F} \frac{d\theta}{ds} - 2(\epsilon + \Sigma_1)\zeta - 2ig\Sigma_I = 0, \quad (29b)$$

$$\hbar v_{2F} \frac{dg}{ds} + 2i\zeta\Sigma_R + 2i\theta\Sigma_I = 0, \quad (29c)$$

where

$$2\Sigma_R = \left( \Sigma_2 e^{-i\alpha} + \Sigma_2^\dagger e^{i\alpha} \right), \quad (30a)$$

$$2i\Sigma_I = \left( \Sigma_2 e^{-i\alpha} - \Sigma_2^\dagger e^{i\alpha} \right). \quad (30b)$$

In the present paper we consider the limit of low tunneling rate  $\Gamma \ll \Delta$  which leads to a small induced gap<sup>17</sup>  $\Delta_{2D} = \Gamma$  and long coherence length  $\xi_{2D} \gg \xi_S$ . We consider an isolated vortex line oriented along the  $Z$  axis perpendicular to the SC/2D interface and choose the gap function inside the bulk SC in the form  $\Delta = \Delta_0(\rho)e^{i\phi}$ , where  $(\rho, \phi)$  are the cylindrical coordinates;  $\Delta_0(\rho)$  approaches the bulk value  $\Delta_\infty$  far from the vortex core. The self energies in the 2D layer, Eqs. (19) or (23), have parts with sharp peaks localized at small distances  $\rho \sim \xi_S$  and the adiabatic long-distance ‘‘vortex potential’’ tail  $\Delta_{2D} \sim \Gamma e^{i\phi}$  at  $\rho \gg \xi_S$  according to Eq. (25).

In the case of clean bulk SC we use the condition of specular reflection at the interface. This can be applied for both coherent and incoherent tunneling models since any possible disorder in tunneling affects only a tiny fraction of bulk electrons whose vast majority reflects without tunneling. For specular reflection, one can use the bulk quasiclassical Green functions obtained for an infinite space. For energies  $\epsilon \ll \Delta_\infty$ , the self energy, Eq. (25)

for long distances ( $\rho \gg \xi_S$ ) is independent of the particular tunneling model and of the disorder in the bulk SC:  $\Sigma_1 \approx 0$ ,  $\Sigma_2 \approx \Gamma e^{i\phi}$ , i.e.,  $\Sigma_R \approx \Gamma s/\rho$ ,  $\Sigma_I \approx \Gamma b/\rho$ . However, the induced vortex potentials close to the primary vortex core are very sensitive to the impurity concentration and momentum exchange during the tunneling process.

For clean bulk SC, the Green function can be parameterized similar to (28) with  $f \rightarrow f_S$ ,  $\zeta \rightarrow \zeta_S$ , and  $\theta \rightarrow \theta_S$ . The Eilenberger equations have the form of Eqs. (29) with  $v_{2F} \rightarrow v_{\parallel} = V_F \cos \chi_p$  where  $\chi_p$  is the polar angle of the momentum, while  $\Sigma_1 = 0$ ,  $\Sigma_2 \rightarrow \Delta = \Delta_0(\rho)e^{i\phi}$ , and  $\Sigma_2^\dagger \rightarrow \Delta^*$ . For energies  $\epsilon \ll \Delta_\infty$  and distances  $s$  of the order or less than the core size, the functions  $g_S$  and  $f_S$  are given in Refs.<sup>23,28</sup>.

$$\zeta_S = \frac{\hbar v_{\parallel} e^{-K}}{2\Lambda [\epsilon - \epsilon_0 \pm i\delta]}, \quad \theta_S = \frac{2}{\hbar v_{\parallel}} \int_0^s \left( \epsilon - \frac{b\Delta_0}{\rho'} \right) \zeta_S ds', \quad (31)$$

$$\epsilon_0(b) = b\Lambda^{-1} \int_0^\infty [\Delta_0/\rho] e^{-K(s)} ds, \quad (32)$$

$$\Lambda = \int_0^\infty e^{-K(s)} ds; \quad K(s) = \frac{2}{\hbar v_{\parallel}} \int_{|b|}^\rho \Delta_0(\rho') d\rho'. \quad (33)$$

For larger distances,  $s \gg \xi_S$ , the function  $\zeta_S$  assumes its asymptotic expression  $\zeta_S^{R(A)} = -b/\rho$  corresponding to the boundary conditions Eq. (25).

#### A. Vortex potentials for coherent tunneling

The vortex potentials induced in the 2D layer crucially depend on the tunneling mechanism. For example, within the coherent tunneling model we get

$$\Sigma_1 = i\Gamma g_S(\mathbf{Q}, \mathbf{r}), \quad \Sigma_2 = i\Gamma f_S(\mathbf{Q}, \mathbf{r})$$

in terms of the infinite-space Green functions, since  $\check{g}_S(+Q_{3z}) = \check{g}_S(-Q_{3z})$  for specular reflection. For energies  $\epsilon \ll \Delta_\infty$  and distances  $s$  of the order or less than the core size  $\xi_S$ , we find from Eq. (28)

$$\Sigma_1 = -\Gamma \zeta_S, \quad (34a)$$

$$\Sigma_2 = \Gamma [\theta_S - i\zeta_S] e^{i\alpha}, \quad (34b)$$

$$\Sigma_2^\dagger = \Gamma [\theta_S + i\zeta_S] e^{-i\alpha}, \quad (34c)$$

where  $\zeta_S$  and  $\theta_S$  are given by Eqs. (31)–(33).

#### B. Vortex potentials for incoherent tunneling

For incoherent tunneling, we find  $\Sigma_1 = i\Gamma \langle g_S \rangle$ ,  $\Sigma_2 = i\Gamma \langle f_S \rangle$  where averaging over the 3D momentum direction is equivalent to the ensemble averaging. To calculate the angular average one can separate the Green functions

into the principal-value part and the delta-functional contribution. For example,

$$g_S^{R(A)} = i\zeta_S^{R(A)} = \wp \frac{i\hbar v_{\parallel} e^{-K}}{2\Lambda [\epsilon - \epsilon_0]} \pm \frac{\pi\hbar v_{\parallel} e^{-K}}{2\Lambda} \delta(\epsilon - \epsilon_0) . \quad (35)$$

Performing averaging over the polar  $\chi_p$  and azimuthal  $\alpha$  angles we take into account the symmetry of the functions under the  $s$ -inversion transformation. As a result, we obtain

$$\Sigma_1 = -\Gamma \langle \zeta_S(s) \rangle , \quad (36)$$

$$\Sigma_2 e^{-i\phi} = \Sigma_2^{\dagger} e^{i\phi} = \Sigma_{ad} + \Sigma_2^{loc} , \quad (37)$$

$$\Sigma_{ad}(\rho) = \wp \langle \Gamma I(s) \text{sign}(s) / 2\Lambda [\epsilon - \epsilon_0] \rangle . \quad (38)$$

We put here

$$I(s) = 2 \int_0^s (\epsilon - \Delta_0 b / \rho) e^{-K(s')} ds' .$$

The off-diagonal components of induced potential are split into the localized and the long-range parts,  $\Sigma_2^{loc}$  and  $\Sigma_{ad}$ , respectively. The long-range function  $\Sigma_{ad}$  can be regarded as an adiabatic induced superconducting gap,  $\Sigma_{ad} \rightarrow \Gamma$  for  $\rho \gg \xi_S$  and  $\Sigma_{ad} \rightarrow 0$  for  $\rho \rightarrow 0$ . Averaging over the azimuthal trajectory angle  $\alpha$  we find:

$$\begin{aligned} \Re \Sigma_2^{loc} &= \Gamma \left\langle \frac{\hbar v_{\parallel} e^{-K}}{2\Lambda \Omega \rho} \left[ 1 - \Re \frac{|\epsilon|}{\sqrt{\epsilon^2 - \Omega^2 \rho^2}} \right] \right\rangle_z , \\ \Im \Sigma_2^{loc} &= \pm \Gamma \left\langle \Re \frac{\epsilon \hbar v_{\parallel} e^{-K}}{2\Lambda \Omega \rho \sqrt{\Omega^2 \rho^2 - \epsilon^2}} \right\rangle_z , \\ \Re \Sigma_1 &= -\text{sign}(\epsilon) \Gamma \left\langle \Re \frac{\hbar v_{\parallel} e^{-K}}{2\Lambda \sqrt{\epsilon^2 - \Omega^2 \rho^2}} \right\rangle_z , \\ \Im \Sigma_1 &= \pm \Gamma \left\langle \Re \frac{\hbar v_{\parallel} e^{-K}}{2\Lambda \sqrt{\Omega^2 \rho^2 - \epsilon^2}} \right\rangle_z . \end{aligned}$$

Here the upper (lower) sign corresponds to a retarded (advanced) self energy term,  $\Omega = d\epsilon_0/db$ , and we use the notation

$$\langle \dots \rangle_z = \frac{1}{2} \int_0^{\pi} (\dots) \sin \chi_p d\chi_p$$

for the average over the polar angle  $\chi_p$  of the 3D Fermi momentum. Note that our calculations are based on the first-order approximation in the small parameter  $b/\rho$ . According to Eq. (30) the symmetrical  $\Sigma_I(-s) = \Sigma_I(s)$  and antisymmetrical  $\Sigma_R(-s) = -\Sigma_R(s)$  parts of the off-diagonal self energy term  $\Sigma_2 e^{-i\phi}$  can be rewritten as  $\Sigma_R = \Sigma_2 e^{-i\phi} s/\rho$  and  $\Sigma_I = \Sigma_2 e^{-i\phi} b/\rho$ .

The self energy obtained above affects the vortex core states in 2D layer in two different ways. The adiabatic part of the induced vortex potential leads to the Andreev localization of QPs with energy smaller than the induced superconducting gap  $\Gamma$  within the induced vortex core at distances of the order of  $\xi_{2D}$ . This forms the CdGM

anomalous branch  $\epsilon_2(b)$  as in an usual superconductor with the corresponding maximum intrinsic gap  $\Gamma$ . Another part of the self energy exponentially decaying at  $\rho \sim \xi_S$  contains information about the CdGM states in the bulk SC; it affects the 2D-layer QP behavior at small scales. The adiabatic large-scale part of the self energy (at  $\rho \gg \xi_S$ ) is universal; it does not depend on the tunneling models and on possible disorder in the bulk SC, while the short-scale induced vortex potential localized at small distances does crucially depend on these factors. Both terms in the induced self energy form the two-scale local DOS (LDOS) radial profile.

#### IV. SCALE SEPARATION METHOD

A natural way to solve Eqs. (29) is to apply the scale separation method. We introduce a distance  $\rho_0$  satisfying  $\xi_S \ll \rho_0 \ll \xi_{2D}$  and consider the Green functions in two overlapping spatial intervals: (i)  $\rho \lesssim \rho_0$  and (ii)  $\rho \gtrsim \rho_0$ . Next we match the solutions in different spatial domains.

##### A. Large distances

At low energies  $\epsilon \ll \Delta_{\infty}$  and large distances  $\rho \gg \xi_S$  the induced vortex potential is given by Eq. (25). QPs propagating along the trajectories with impact parameters  $b > \xi_S$  that miss the primary vortex core are affected only by this long-distance ( $\xi_{2D} \gg \xi_S$ ) part of the induced gap potential. In the low energy limit  $\epsilon < \Gamma \ll \Delta_{\infty}$  the appropriate boundary conditions far from the induced vortex core ( $\rho \gg \xi_{2D}$ ) are

$$\theta = \frac{\Gamma s / \rho}{\sqrt{\Gamma^2 - \epsilon^2}} , \quad \zeta = \frac{-\Gamma b / \rho}{\sqrt{\Gamma^2 - \epsilon^2}} , \quad g = \frac{-i\epsilon}{\sqrt{\Gamma^2 - \epsilon^2}} . \quad (39)$$

For both tunneling models and arbitrary disorder rate inside the superconductor and for  $\rho \gg \xi_S$  Eqs. (29) take the form:

$$\hbar v_{2F} \frac{d\zeta}{ds} + 2\epsilon\theta - 2ig\Gamma s/\rho = 0 , \quad (40a)$$

$$\hbar v_{2F} \frac{d\theta}{ds} - 2\epsilon\zeta - 2ig\Gamma b/\rho = 0 , \quad (40b)$$

$$\hbar v_{2F} \frac{dg}{ds} + 2i\theta\Gamma b/\rho + 2i\zeta\Gamma s/\rho = 0 . \quad (40c)$$

The functions  $g$  and  $\zeta$  are even in  $s$  while  $\theta$  is odd, so we can consider only positive  $s$  values. We obtain the solution of the above equations using the first-order perturbation theory in the impact parameter  $b$ :  $\tilde{w}(s) = \tilde{w}_0(s) + \tilde{w}_1(s)$ , where  $\tilde{w}(s) = (\zeta, \theta, ig)^T$ . As we shall see later, this approximation holds for  $|b| \ll \xi_{2D}$ . The zero order in  $b$  solution reads

$$\tilde{w}_0(s) = \frac{1}{\sqrt{\Gamma^2 - \epsilon^2}} \tilde{w}_0(s) + \frac{C}{\sqrt{\Gamma^2 - \epsilon^2}} \tilde{w}_-(s) , \quad (41)$$

where

$$\tilde{u}_{\pm}(s) = \begin{pmatrix} \sqrt{\Gamma^2 - \epsilon^2} \\ \pm\epsilon \\ \pm\Gamma \end{pmatrix} e^{\pm\lambda s}, \quad \tilde{u}_0(s) = \begin{pmatrix} 0 \\ \Gamma \\ \epsilon \end{pmatrix}$$

and  $\lambda = 2\sqrt{\Gamma^2 - \epsilon^2}/\hbar v_{2F}$ . This solution satisfies the boundary conditions  $g = -i\epsilon/\sqrt{\Gamma^2 - \epsilon^2}$ ,  $\zeta = 0$  and  $\theta = \Gamma/\sqrt{\Gamma^2 - \epsilon^2}$  for  $s \rightarrow \infty$  and  $\epsilon^2 < \Gamma^2$ . The first order correction  $\tilde{w}_1$  can be written as

$$\tilde{w}_1(s) = \frac{C_0(s)\tilde{u}_0}{\sqrt{\Gamma^2 - \epsilon^2}} + \frac{C_+(s)\tilde{u}_+}{\sqrt{\Gamma^2 - \epsilon^2}} + \frac{C_-(s)\tilde{u}_-}{\sqrt{\Gamma^2 - \epsilon^2}}, \quad (42)$$

where

$$\xi_{2D}C_0(s) = 2Cb \int_s^\infty e^{-\lambda s} \frac{ds}{\rho}, \quad (43a)$$

$$\xi_{2D}C_+(s) = -b \int_s^\infty e^{-\lambda s} \frac{ds}{\rho}, \quad (43b)$$

$$\xi_{2D}C_-(s) = -b \int_{s_c}^s e^{\lambda s} \frac{ds}{\rho}. \quad (43c)$$

The lower limit of integration in  $C_-$ ,  $s_c$ , has to be taken as  $s_c \sim \xi_S$  for trajectories that go through the primary vortex core,  $b \lesssim \xi_S$ , so that the logarithmic divergence is cut off at the distances  $\sim \xi_S$  where the long-range vortex potential  $\Sigma_{ad}$  (38) vanishes. For  $b \gg \xi_S$  we have  $s_c = 0$ . The perturbation approach holds as long as  $C_0 \ll C$  and  $C_+ \ll 1$ , i.e., as long as  $|b| \ll \xi_{2D}$ . For  $s \gg \xi_{2D}$  the coefficient  $C_0$  decays faster than exponentially, while

$$C_+(s)e^{\lambda s} \rightarrow C_-(s)e^{-\lambda s} \rightarrow -\frac{\Gamma}{2\sqrt{\Gamma^2 - \epsilon^2}} \frac{b}{\rho}$$

so that  $\zeta$  approaches  $-(b/\rho)\Gamma/\sqrt{\Gamma^2 - \epsilon^2}$  and the corrections to  $\theta$  and  $g$  vanish as it should be according to (39). For a small distance  $s = s_0$  defined as  $\rho_0^2 = s_0^2 + b^2$  we have

$$\zeta(s_0) = C + C_+(s_0) + C_-(s_0), \quad (44a)$$

$$\theta(s_0) = \frac{1}{\sqrt{\Gamma^2 - \epsilon^2}} \{ \Gamma - \epsilon C + \Gamma C_0(s_0) + \epsilon [C_+(s_0) - C_-(s_0)] \}, \quad (44b)$$

$$g(s_0) = \frac{i}{\sqrt{\Gamma^2 - \epsilon^2}} \{ -\epsilon + \Gamma C - \epsilon C_0(s_0) - \Gamma [C_+(s_0) - C_-(s_0)] \}. \quad (44c)$$

## B. Matching for large impact parameters

Far from the primary vortex core at impact parameters  $\xi_S \ll b \ll \xi_{2D}$  the perturbation result Eqs. (40) can be applied along the entire trajectory so that one can put  $s_0 = s_c = 0$ . The boundary condition for an odd function requires  $\theta(0) = 0$ . Since in this case  $C_-(0) = 0$ , we find from Eq. (44b)

$$\Gamma + \epsilon C_+(0) = \epsilon C - \Gamma C_0(0).$$

Expressing the coefficients  $C_0$  and  $C_+$  in terms of the energy

$$\epsilon = \epsilon_2(b) = \frac{2\Gamma^2 b}{\hbar v_{2F}} \ln \eta, \quad (45)$$

of bound states in the induced vortex core, with  $\eta = \xi_{2D}/|b|$ ,  $C_0 = -2CC_+ = C\epsilon_2(b)/\Gamma$ , we find

$$C[\epsilon - \epsilon_2(b)] = \Gamma - \epsilon\epsilon_2(b)/2\Gamma. \quad (46)$$

According to Eq. (46)  $\epsilon_2(b)$  is the only spectrum branch in the energy interval  $|\epsilon| \ll \Delta_\infty$ . The Green function is

$$g(s) = \frac{-i\epsilon}{\sqrt{\Gamma^2 - \epsilon^2}} + \frac{i\Gamma C}{\sqrt{\Gamma^2 - \epsilon^2}} e^{-\lambda s} - \frac{i\epsilon C_0(s)}{\sqrt{\Gamma^2 - \epsilon^2}} - \frac{i\Gamma}{\sqrt{\Gamma^2 - \epsilon^2}} [C_+(s)e^{\lambda s} - C_-(s)e^{-\lambda s}]. \quad (47)$$

For  $s \gg \xi_{2D}$  we have  $C_0 \rightarrow 0$ ,  $C_+e^{\lambda s} - C_-e^{-\lambda s} \rightarrow 0$ , so that the first term is the homogeneous background while the rest terms describe the vortex contribution. To obtain the retarded function for  $\epsilon^2 > \Gamma^2$  one has to continue  $\sqrt{\Gamma^2 - \epsilon^2}$  analytically throughout the upper half-plane of complex  $\epsilon$  keeping  $\Re\sqrt{\Gamma^2 - \epsilon^2} > 0$ .

## C. Matching for small impact parameters

To find the Green functions for small impact parameters  $b \lesssim \xi_S$  one has to match Eqs. (44) with the solution obtained in the vortex core region. For small  $s < s_0$  we assume that the even parts of the Green function  $g(s)$  and  $\zeta(s)$  are nearly constant in the interval  $0 < s < s_0$ . Integrating Eq. (29b) over  $s$  from 0 to  $s_0$  along the trajectory we find the matching condition

$$\frac{\hbar v_{2F}}{2} \theta(s_0) = \zeta(s_0) \int_0^{s_0} \Sigma_1 ds + ig(s_0) \int_0^{s_0} \Sigma_I ds. \quad (48)$$

Equation (48) determines the constant  $C$ . Its poles define the eigenstates of excitations as functions of energy and the impact parameter. While deriving the effective boundary condition (48) for  $b \lesssim \xi_S$ , one needs to separate the exponentially converging parts  $\Sigma_{1,I}^{loc}$  at  $s \sim \xi_S$  from the long-distance,  $s \gg \xi_S$ , asymptotics of  $\Sigma_{1,I}$ . For  $\epsilon \ll \Delta_\infty$  the long-distance expressions, Eq. (25), yield  $\Sigma_1 \rightarrow 0$ ,  $\Sigma_I \rightarrow \Gamma b/\rho$ . Therefore,

$$\begin{aligned} \int_0^{s_0} \Sigma_I ds &= \int_0^{\xi_S} \Sigma_I^{loc} ds + \Gamma \int_{\xi_S}^{s_0} b/\rho ds \\ &\approx \int_0^\infty \Sigma_I^{loc} ds + \Gamma b \ln(s_0/\xi_S). \end{aligned} \quad (49)$$

while  $\int_0^{s_0} \Sigma_1 ds$  can be extended to infinity. The localized self energy parts  $\Sigma_1$ ,  $\Sigma_I^{loc}$  determine the small-distance LDOS and spectrum of excitations and depend on the particular tunneling mechanism.

## V. MULTIPLE VORTEX CORE IN THE CLEAN LIMIT. QUASIPARTICLE SPECTRUM AND DENSITY OF STATES.

### A. Isotropic Fermi surface

In this section we consider an idealized picture without any disorder. For large impact parameters,  $b \gg \xi_S$ , the corresponding solutions for the Green functions, Eq. (47), coincide with the standard CdGM expressions where the gap value is replaced with  $\Gamma$ . The corresponding anomalous spectrum for 2D excitations is given by Eq. (45).<sup>23,28</sup> This modified CdGM branch dominates in the LDOS at large distances  $\rho \gg \xi_S$ .

The normalized LDOS is defined as an average over the trajectories:

$$N(\mathbf{r}, \epsilon) = \int_0^{2\pi} N_\epsilon(s, b) \frac{d\alpha'}{2\pi} = \int_{-\rho}^{\rho} \frac{N_\epsilon(\sqrt{\rho^2 - b^2}, b)}{\sqrt{\rho^2 - b^2}} \frac{db}{\pi}$$

where  $N_\epsilon(s, b) = [g^R(s, b) - g^A(s, b)]/2$ ,  $s = \rho \cos \alpha'$ , and  $b = -\rho \sin \alpha'$ . For  $|\epsilon| < \Gamma$ , a nonzero LDOS comes only from the vortex contribution of the second and third terms in (47) due to the presence of a pole in the coefficient  $C$  according to Eq. (46). The Green functions and LDOS reach their long-distance values  $g = -i\epsilon/\sqrt{\Gamma^2 - \epsilon^2}$  and  $N = \Re|\epsilon|/\sqrt{\epsilon^2 - \Gamma^2}$  as  $\rho \rightarrow \infty$ . For  $\rho \gg \xi_S$  the trajectories with large impact parameters  $b \gtrsim \xi_S$  give the main contribution to the LDOS. In the region  $\xi_S \ll \rho \ll \xi_{2D}$  we get the angle-resolved density of states in the form:

$$N_\epsilon(s, b) = \frac{\sqrt{\Gamma^2 - \epsilon^2}(\Gamma^2 - \epsilon^2/2)}{\Gamma^2} \times \pi \delta[\epsilon - \epsilon_2(b)], \quad |\epsilon| < \Gamma \quad (50)$$

$$N_\epsilon(s, b) = \frac{\sqrt{\epsilon^2 - \Gamma^2}[\Gamma^2 - \epsilon_2^2(b)/2]}{\text{sign}(\epsilon)\Gamma^2[\epsilon - \epsilon_2(b)]}, \quad |\epsilon| > \Gamma. \quad (51)$$

Thus, the corresponding LDOS in the energy interval  $|\epsilon| < \Gamma$  has the only peaks at  $\epsilon = \epsilon_2(\pm\rho)$ :

$$N(\rho, \epsilon) = \frac{1}{\pi} \int_{-\rho}^{\rho} N_\epsilon(\sqrt{\rho^2 - b^2}, b) \frac{db}{\sqrt{\rho^2 - b^2}} = \Re \frac{\sqrt{\Gamma^2 - \epsilon^2}(1 - \epsilon^2/2\Gamma^2)}{\sqrt{\epsilon_2^2(\rho) - \epsilon^2}}. \quad (52)$$

For energies above the induced gap,  $|\epsilon| > \Gamma$ , for the same distances the LDOS is monotonically increasing with  $|\epsilon|$  to its normal state value:

$$N(\rho, \epsilon) = \sqrt{\epsilon^2 - \Gamma^2} \left[ \frac{|\epsilon|}{2\Gamma^2} + \frac{(1 - \epsilon^2/2\Gamma^2)}{\sqrt{\epsilon^2 - \epsilon_2^2(\rho)}} \right]. \quad (53)$$

A trajectory with a small impact parameter  $b \lesssim \xi_S$  can be divided into the part far from the primary vortex core, and the region inside the core. Far from the core

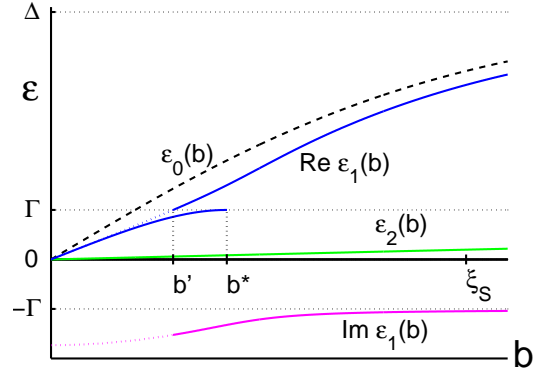


FIG. 5: (Color online) Two localized branches,  $\epsilon_1(b)$  and  $\epsilon_2(b)$  of the spectrum, Eq. (59), in the limit of coherent tunneling, for  $\epsilon < \Gamma$ .  $b^*$  is defined as  $\epsilon_1(b^*) = \Gamma - 0$ , while  $b'$  corresponds to  $\Re \epsilon_1(b') = \Gamma + 0$ . The spectrum satisfies  $\epsilon_{1,2}(-b) = -\epsilon_{1,2}^*(b)$ .

the solution is found using the vortex potentials Eq. (25). The self energies of the primary vortex in Eq. (18) have poles at the usual CdGM energy  $\epsilon_0(b)$  with the corresponding wave functions exponentially localized within  $\rho \sim \xi_S$  and regular parts extending over large distances  $\rho \rightarrow \pm\infty$ <sup>23,28</sup>:

$$\Sigma_R = \Gamma\theta_S, \quad \Sigma_I = -\Gamma\zeta_S. \quad (54)$$

Note that the localized part  $\Sigma_2^{loc}$  of the effective order parameter  $\Sigma_2$  has the coordinate dependence  $\Sigma_2^{loc} = i\Sigma_I^{loc}(b, s)e^{i\alpha}$  with *zero* circulation, unlike its adiabatic part (25)  $\Sigma_2(\rho \gg \xi_S) = \Gamma e^{i\phi}$ . As we will see below it is this different angular dependence of the effective gap asymptotics, which leads to the formation of a “shadow” of the bulk SC anomalous branch in the excitation spectrum and LDOS in the 2D layer.

Using Eqs. (43) for the long-distance part of the trajectory we find

$$C_0(s_0) = \frac{2Cb}{\xi_{2D}} \ln \frac{1}{\lambda s_0}, \quad (55a)$$

$$C_+(s_0) \pm C_-(s_0) \approx -\frac{b}{\xi_{2D}} \ln \frac{1}{\lambda \xi_S} \approx -\frac{\epsilon_2(b)}{2\Gamma}. \quad (55b)$$

We now match the asymptotic solution Eqs. (44) obtained for  $s \geq s_0$  with the solution for the short-distance part of the trajectory, Eqs. (34) and (31) - (33), using Eq. (48) and Eq. (49). As a result,

$$C \left[ \xi_{2D}[\epsilon - \epsilon_2(b)] + 2[\Gamma - \sqrt{\Gamma^2 - \epsilon^2} - \frac{\epsilon\epsilon_2(b)}{\Gamma}] \int_0^\infty \zeta_0 ds \right] = \left[ \xi_{2D}\Gamma + 2\epsilon \int_0^\infty \zeta_0 ds - \xi_{2D} \frac{\epsilon\epsilon_2(b)}{2\Gamma} - (\Gamma + \sqrt{\Gamma^2 - \epsilon^2}) \frac{\epsilon_2(b)}{\Gamma} \int_0^\infty \zeta_0 ds \right], \quad (56)$$

where  $\zeta_0(s)$  is the localized part of  $\zeta_S$  and

$$\int_0^\infty \zeta_0 ds = \frac{\hbar v_{||}}{2[\epsilon - \epsilon_0(b)]}. \quad (57)$$

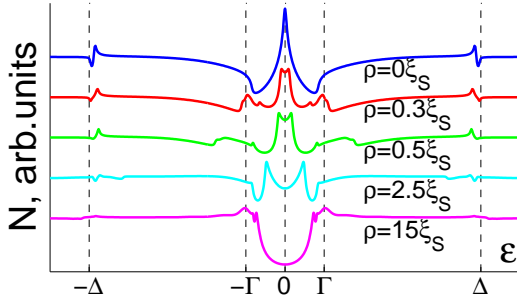


FIG. 6: (Color online) LDOS in logarithmic scale for coherent tunneling in the clean limit. Curves, taken for different distances  $\rho$  from the vortex center, are vertically shifted for clarity. The peaks in LDOS exist up to distances  $\sim \xi_{2D}$ . Here  $\Delta/\Gamma = 5$ ,  $q_v = 1$ .

Here we put  $g = i\zeta_0$  and replace the cutoff parameter in (45) by  $\eta = \xi_{2D}/\xi_S$ . For  $b \gg \xi_S$  the contributions from the primary vortex core proportional to  $\int_0^\infty \zeta_0 ds$  vanish since the trajectory misses the core, and Eq. (56) goes over into Eq. (46).

For small  $b \ll \xi_{2D}$  the Green function has a pole when

$$P(\epsilon, b) = [\epsilon - \epsilon_2(b)][\epsilon - \epsilon_0(b)] + q_v \left[ \Gamma^2 - \Gamma \sqrt{\Gamma^2 - \epsilon^2} - \epsilon \epsilon_2(b) \right] = 0 \quad (58)$$

where  $q_v = v_{\parallel}/v_{2F}$ . One can show that including the higher order terms in the parameter  $\epsilon_2(b)/\Gamma$  the corresponding energy dispersion relation takes the form:

$$\frac{[\epsilon - \epsilon_2(b)][\epsilon - \epsilon_0(b)]}{\Gamma q_v} + \Gamma - \sqrt{\Gamma^2 - [\epsilon - \epsilon_2(b)]^2} = 0 \quad (59)$$

For  $b \lesssim \xi_S$ , the cutoff parameter in Eq. (45) should be replaced with  $\eta = \xi_{2D}/\xi_S$ .

The resulting two-scale spectrum is shown in Fig. 5. There are two real-valued branches in the range  $|\epsilon| < \Gamma$  crossing zero of energy as functions of the impact parameter and one complex-valued branch in the range  $\Gamma < |\epsilon| < \Delta_\infty$ . The lowest-energy branch  $\epsilon_2(b)$  has a scale  $\xi_{2D}$  as a function of the impact parameter: For  $b \lesssim \xi_{2D}$  it is given by Eq. (45) with the proper cutoff parameter  $\eta$  as discussed above and saturates at  $\epsilon = \Gamma$  for  $b \gg \xi_{2D}$ . The branch  $\epsilon_1(b)$  has a scale  $\xi_S$ : For  $\epsilon < \Gamma$  it goes slightly below the CdGM spectrum  $\epsilon_0(b)$  of the bulk SC,  $\epsilon_1(b) = (1 + q_v/2)^{-1} \epsilon_0(b)$ . Above  $\Gamma$  the spectrum transforms into a scattering resonance due to the decay into delocalized modes propagating in the 2D layer:  $\epsilon_1(b) = \epsilon_0(b) - i\Gamma q_v$  for  $|\epsilon| \gg \Gamma$ . Since Eq. (59) determines a pole of the retarded Green function in the lower half-plane of complex  $\epsilon$ , the square root in Eq. (59) should be analytically continued through the cut going from  $-\infty$  to  $-\Gamma$  and from  $\Gamma$  to  $+\infty$ . As a result,  $\epsilon_1(b)$  has a discontinuity at  $\epsilon_1 = \Gamma$  with  $b'/\xi_S \approx 0.29$  and  $b^*/\xi_S \approx 0.42$ .

The two branches appear due to the presence of two sub-systems, the bulk SC and the 2D proximity layer,

each with its own anomalous branch. The existence of two anomalous branches follows also from the index theorem<sup>29,30</sup>. Indeed, its application requires that both zero of the quasiclassical Hamiltonian at the Fermi surface and its singularity at  $\epsilon = \epsilon_0(b)$  are taken into account when calculating the topological invariant. As a result, the number of anomalous branches is increased up to 2 for a single-quantum vortex.

The multiple-branch spectrum results in multiple-peak structure in the LDOS (Fig. 6), which appears to be most pronounced deeply inside the primary core (at distances  $\rho \lesssim \xi_S^2/\xi_{2D}$  when  $\epsilon_1 < \Gamma$ ) thus illustrating the two-scale structure of the vortex core. The LDOS is obtained from the angle-resolved DOS (normalized by its normal state value)  $N_\epsilon(s, b) = [g^R(s, b) - g^A(s, b)]/2$  averaged over the trajectory direction.

The angle-resolved DOS for small energies  $|\epsilon| \ll \Gamma$  and  $\rho \lesssim \xi_S$  reads

$$N_\epsilon(s, b) = \frac{\pi \Gamma q_v}{2} \delta[\epsilon - \epsilon_1(b)] + \frac{\pi \Gamma (q_v + 2)}{2} \delta[\epsilon - \epsilon_2(b)]. \quad (60)$$

Here we neglect the terms  $\epsilon \epsilon_2(b)/\Gamma^2$  and  $\epsilon_2(b)/\epsilon_1(b)$  and put  $\epsilon_0(b)/\epsilon_1(b) = 1 + q_v/2$  according to low energy asymptotics. In this case the LDOS

$$N(\rho, \epsilon) = \Re \frac{\Gamma q_v}{2\sqrt{\epsilon_1^2(\rho) - \epsilon^2}} + \Re \frac{\Gamma (q_v + 2)}{2\sqrt{\epsilon_2^2(\rho) - \epsilon^2}} \quad (61)$$

reveals a two-peak structure vs energy at  $\epsilon = \epsilon_{1,2}(\rho)$ . For  $|\epsilon| \sim \Gamma$ , one can neglect  $\epsilon_2(b)$  and obtain:

$$[\epsilon - \epsilon_0(b)] \left[ \Gamma + \sqrt{\Gamma^2 - \epsilon^2} \right] + q_v \Gamma \epsilon = 0. \quad (62)$$

For  $|\epsilon| > \Gamma$  the dispersion relation is complex valued and for retarded functions takes the form:

$$\epsilon[\epsilon - \epsilon_0(b)] + q_v \Gamma \left[ \Gamma + i \text{sign}(\epsilon) \sqrt{\epsilon^2 - \Gamma^2} \right] = 0. \quad (63)$$

The latter equation describes the resonant states in the 2D vortex core which decay into the QP waves propagating in the 2D layer above the induced gap.

Finally, the whole spectrum structure, shown in Fig. 5, has two anomalous branches: (i) one of them  $\epsilon_2(b)$  is completely real-valued and follows the CdGM spectrum for the superconductor with homogeneous gap  $\Gamma$ ; (ii) another one is close to the bulk CdGM spectrum, but has a discontinuity at  $\epsilon = \Gamma$ , where it becomes essentially complex.

Thus, the LDOS for energies above the induced gap  $|\epsilon| > \Gamma$  and small distances  $\rho, b \lesssim \xi_S$  reads

$$N(\rho, \epsilon) = \frac{\sqrt{\epsilon^2 - \Gamma^2}}{|\epsilon|} + \frac{q_v \Gamma^2}{2|\epsilon|} \times \Re \frac{\sqrt{\epsilon^2 - \Gamma^2} - i\Gamma}{\sqrt{(\epsilon^2 + q_v \Gamma^2 + i q_v \Gamma \sqrt{\epsilon^2 - \Gamma^2})^2 - \epsilon^2 \epsilon_0^2(\rho)}} \quad (64)$$

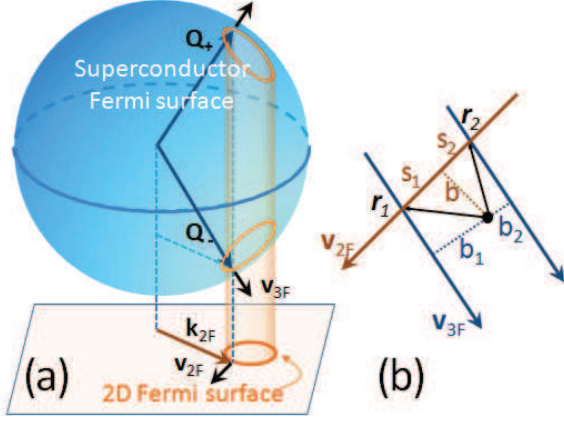


FIG. 7: (a) An example of anisotropic Fermi surfaces showing a spherical 3D Fermi surface on top of a part of a 2D Fermi surface in the layer shifted from the center of its Brillouin zone. The closed loops show the 2D Fermi line and its projections onto the 3D Fermi surface. The directions of the 3D Fermi velocity projection  $\mathbf{v}_{3F}$  on the plane  $z = 0$  in the bulk does not coincide with that in the 2D layer,  $\mathbf{v}_{2F}$ . (b) Different points  $\mathbf{r}_1$  and  $\mathbf{r}_2$  specified by  $s_1$  and  $s_2$  on a 2D trajectory with given impact parameter  $b$  belong to trajectories in 3D with different impact parameters  $b_1$  and  $b_2$ .

and has the only peak at  $\epsilon = \Re\epsilon_1(\rho)$  of the height  $\sim \Gamma^2/\epsilon_0^2(\rho)$  for  $\rho \gtrsim \xi_S^2/\xi_{2D}$ . In the opposite limit of rather large distances  $\rho > \xi_S^2/\xi_{2D}$  at  $|\epsilon| > \Gamma$ , the spectrum reduces to the CdGM spectrum with a finite broadening:

$$\epsilon_1(b) = \epsilon_0(b) - i\Gamma q_v. \quad (65)$$

The LDOS has a small difference from its normal state value  $N_0 = 1$ :

$$N(\rho, \epsilon) = 1 + \frac{q_v \Gamma^2}{2\epsilon^2} \Re \frac{|\epsilon| - i\Gamma}{\sqrt{(\epsilon + iq_v \Gamma)^2 - \epsilon_0^2(\rho)}} \quad (66)$$

The LDOS in the whole energy range (61, 64) has two or even three peaks for such distances. The latter case is realized at the distances corresponding to  $b' < b < b^*$ , where the spectrum vs the impact parameter has 3 anomalous branches.

The numerical LDOS patterns have been obtained by the subsequent solving of the two sets of Eilenberger equations in the Riccati parametrization<sup>31</sup>: first, we calculate the Green functions in the bulk SC using the approximation  $\Delta_0(\rho) = \Delta_\infty \rho / \sqrt{\rho^2 + \xi_S^2}$  and next we solve Eq. (18) in the 2D layer using Eq. (19).

## B. Anisotropic Fermi surface

Here we briefly discuss the effects of anisotropic Fermi surfaces in 3D and/or 2D systems. We will be interested only in main distinctions which the anisotropy causes within the coherent tunneling model as compared to the isotropic case considered above. For anisotropic surfaces,

one can also apply the method of scale separation in the same manner as we did it in Sec. IV. The consideration for the region of large impact parameters does not differ significantly, such that the solution for the Green functions together with the matching conditions look similar to Eqs. (41), (43), (55) and (48), (49). However, the region of small impact parameters of the order of  $\xi_S$  gives an essentially different result. The main distinction is that the directions of QP trajectories which are determined by the group velocities  $\partial\epsilon_{2D}/\partial\mathbf{k}$  and  $\partial\epsilon_{3D}/\partial\mathbf{Q}$  for given in-plane momentum in 2D and 3D systems do not coincide, Fig. 7(a). As a result, the integral in Eq. (48) along a 2D trajectory involves trajectories with different impact parameters used to parameterize the 3D Green functions, see Fig. 7(b). Within the quasiclassical approximation, the integral will thus give an imaginary part which comes from the delta function at the 3D core spectrum and a real contribution from a smooth dependence. The spectrum  $\epsilon_2(b)$  at small impact parameters thus becomes broadened and shifted from its initial position. The imaginary contribution appears due to the coupling of the QP trajectory in the 2D layer with a quasiclassical continuum of trajectories inside the superconductor corresponding to different impact parameters. This coupling results from the non-conservation of the angular momentum in the anisotropic system. The imaginary contribution will be also present if the primary-core spectrum is broadened by disorder or inelastic scattering. The situation is in many respects similar to that for incoherent tunneling model discussed in the following section. Of course, attributing the origin of the imaginary part of energy for the anisotropic case to the continuum of states in the bulk SC, we ignore the angular momentum quantization in the primary vortex core. The true quantum mechanical consideration accounting for the level quantization could possibly change this conclusion and lead to a real-valued energy spectrum for ideal systems without disorder.

In this Section we consider the low-energy behavior of the Green function at small impact parameters,  $b \ll \xi_S$  where the spectral energy  $\epsilon_2(b)$  is very small and can be neglected. We assume that the trajectories in the bulk SC and in the 2D layer do not coincide; the Fermi velocities  $\mathbf{v}_{2F}$  and  $\mathbf{v}_{3F}$  are at an angle  $\delta\alpha$  to each other, see Fig. 7(b). The impact parameter  $b_S$  and trajectory coordinate  $s_S$  in the superconductor are coupled with the ones in the 2D layer ( $b$  and  $s$ ) through

$$\begin{aligned} b_S &= \rho \sin(\phi - \alpha + \delta\alpha) = b \cos \delta\alpha + s \sin \delta\alpha, \\ s_S &= \rho \cos(\phi - \alpha + \delta\alpha) = s \cos \delta\alpha - b \sin \delta\alpha. \end{aligned}$$

As we know, at small distances  $\rho \ll \xi_S$  the part  $\zeta_S$  of anomalous Green function  $f_S$  in the bulk superconductor is large compared with  $\zeta_S \gg \theta_S$ . Neglecting the latter, we have for the self energies in Eq. (30):

$$\Sigma_R = \Sigma_1 \sin \delta\alpha, \quad (67a)$$

$$\Sigma_I = \Sigma_1 \cos \delta\alpha, \quad (67b)$$

The diagonal self energy is  $\Sigma_1 = i\Gamma g_S \approx -\Gamma\zeta_S$ . Note that the self energies depend on trajectory coordinate  $s$  in 2D layer through the impact parameter  $b_S = b \cos \delta\alpha + s \sin \delta\alpha$  in the bulk superconductor and do not possess definite symmetry in  $s$ . Therefore, one needs to consider the region inside the primary core more carefully allowing for contributions from even and odd components of the corresponding functions.

As in Sec. IV we use the scale separation method and subdivide a 2D layer trajectory with a small impact parameter  $b \lesssim \xi_S$  into the long-distance part far from the primary vortex core, and the region inside the core. We introduce a distance  $\rho'$  satisfying  $\xi_S \ll \rho' \ll \xi_{2D}$  and consider the Green functions in two overlapping spatial intervals: (i)  $\rho \lesssim \rho'$  and (ii)  $\rho \gtrsim \rho'$ . Next we match the solutions in different spatial domains. Far from the core the solution is found using the vortex potentials Eq. (25).

In the region inside the primary vortex core the self energies play the most important role. Using the approximation (67),  $\Sigma_R = \Sigma_1 \sin \delta\alpha$ ,  $\Sigma_I = \Sigma_1 \cos \delta\alpha$  and neglecting  $\epsilon$ , Eqs. (29) at small distances  $s < s_0$  can be written in the matrix form

$$\frac{d}{ds} \tilde{w} + \frac{2\Sigma_1}{\hbar v_{2F}} \tilde{A} \tilde{w} = 0. \quad (68)$$

As in Sec. IV we use the vector  $\tilde{w} = (\zeta, \theta, ig)^T$ . The constant matrix

$$\tilde{A} = \begin{pmatrix} 0 & 1 & -\sin \delta\alpha \\ -1 & 0 & -\cos \delta\alpha \\ -\sin \delta\alpha & -\cos \delta\alpha & 0 \end{pmatrix}$$

has threefold degenerated zero eigenvalue, therefore the solution of Eq. (68) can be written in terms of mutually orthogonal eigenvector  $\tilde{v}_0 = (-\cos \delta\alpha, \sin \delta\alpha, 1)^T$  and adjoined vectors  $\tilde{v}_1 = (-\sin \delta\alpha, -\cos \delta\alpha, 0)^T$  and  $\tilde{v}_2 = (\cos \delta\alpha, -\sin \delta\alpha, 1)^T$ :

$$\tilde{w} = C_0(s)\tilde{v}_0 + C_1(s)\tilde{v}_1 + C_2\tilde{v}_2, \quad (69)$$

where  $\tilde{A}\tilde{v}_0 = 0$ ,  $\tilde{A}\tilde{v}_1 = \tilde{v}_0$ , and  $\tilde{A}\tilde{v}_2 = 2\tilde{v}_1$ . Therefore

$$\frac{dC_1(s)}{dx} = -2\frac{2\Sigma_1(s)}{\hbar v_{2F}} C_2, \quad (70a)$$

$$\frac{dC_0(s)}{dx} = -\frac{2\Sigma_1(s)}{\hbar v_{2F}} C_1(s). \quad (70b)$$

The solution is

$$C_1 = C_1^0 + 2C_2 I(s), \quad C_0 = C_0^0 + C_1^0 I(s) + C_2 I(s)^2, \quad (71)$$

where  $\Sigma_1 = -\Gamma\zeta_S$  and

$$I(s) = \frac{2\Gamma}{\hbar v_{2F}} \int_0^s \zeta_S(s') ds'. \quad (72)$$

The three equations (68) are not independent because of the normalization  $g^2 + \zeta^2 + \theta^2 = 1$ . Therefore, the three coefficients  $C_1^0$ ,  $C_2$ , and  $C_0^0$  are coupled through  $(C_1^0)^2 = 4C_2 C_0^0$ .

Multiplying Eq. (69) by the vectors  $\tilde{v}_2^+$  and  $\tilde{v}_1^+$  and using Eq. (71) one can obtain 4 conditions at  $s = \pm s_0$

$$(\zeta \cos \delta\alpha - \theta \sin \delta\alpha + ig)_{\pm s_0} = C_2, \quad (73a)$$

$$(\zeta \sin \delta\alpha + \theta \cos \delta\alpha)_{\pm s_0} = -C_1^0 - 2C_2 I(\pm s_0) \quad (73b)$$

Excluding the coefficients  $C_2$  and  $C_1^0$  we find

$$[\zeta \cos \delta\alpha - \theta \sin \delta\alpha + ig]_{s_0} = 0, \quad (74a)$$

$$[\zeta \sin \delta\alpha + \theta \cos \delta\alpha]_{s_0} + 2I_{\text{odd}} \{\zeta \cos \delta\alpha - \theta \sin \delta\alpha + ig\}_{s_0} = 0, \quad (74b)$$

where the integral  $I(s) = I_{\text{even}}(s) + I_{\text{odd}}(s)$  in Eq. (72) separated into even  $I_{\text{even}}(-s) = I_{\text{even}}(s)$  and odd  $I_{\text{odd}}(-s) = -I_{\text{odd}}(s)$  parts and  $[x]_{s_0} = x(s_0) - x(-s_0)$  and  $\{x\}_{s_0} = x(s_0) + x(-s_0)$ . The integral

$$I_{\text{odd}} = \frac{\Gamma}{\hbar v_{2F}} \int_{-s_0}^{s_0} \zeta_S(s') ds'$$

takes the form

$$I_{\text{odd}} = \frac{\Gamma v_{\parallel}}{v_{2F} 2\Lambda \sin \delta\alpha} \mathcal{P} \int_{-\infty}^{\infty} \frac{e^{-K(z \cot \delta\alpha - b \sin \delta\alpha)}}{[\epsilon - \epsilon_0(b \cos \delta\alpha + z)]} dz \mp \frac{i\pi v_{\parallel} \Gamma}{2\Lambda v_{2F} \Omega \sin \delta\alpha} \exp \left[ -K \left( \frac{\epsilon \cot \delta\alpha}{\Omega} - \frac{b}{\sin \delta\alpha} \right) \right], \quad (75)$$

where we put  $s \sin \delta\alpha = z$ . The second term comes from the delta-function contribution at one of the primary core states, see Eq. (31); the upper (lower) sign corresponds to retarded (advanced) function. For  $\delta\alpha \lesssim \epsilon/\Delta$  the second term disappears while the first gives the real pole contribution which is equivalent to Eq. (57). One concludes that the imaginary part disappears only for trajectories which are almost parallel (within an angle  $\delta\alpha \lesssim \epsilon/\Delta$ ). For  $\delta\alpha \gg \epsilon/\Delta$  the first (real) term vanishes since the expression under the integral becomes odd in  $z$ . Note that for  $\epsilon = 0$  and  $b = 0$  the real term vanishes exactly.

Equations (74) are the matching conditions with the solution in the large-distance region,  $s > s_0$ . They are generalizations of the matching condition Eq. (48) derived earlier for the isotropic situation. The two conditions Eqs. (74) determine the even and odd parts of the Green functions.

The long-distance solution is found in the same way as in Sec. IV. However, it does no longer have a definite symmetry with respect to  $s \rightarrow -s$ . We separate the even and odd components  $\tilde{w} = \tilde{w}_{\text{even}} + \tilde{w}_{\text{odd}}$  and consider both  $s > 0$  and  $s < 0$ . In this Section we only discuss the behavior of the Green function for low energies and small impact parameter. We thus neglect the corrections to  $\tilde{w}$  proportional to  $b/\xi_{2D}$ . In this case  $\tilde{w}_{\text{even}}$  is given by Eq. (41) where now

$$\tilde{u}_{\pm}(s) = \begin{pmatrix} \sqrt{\Gamma^2 - \epsilon^2} \\ \pm \epsilon \text{sign}(s) \\ \pm \Gamma \end{pmatrix} e^{\pm \lambda |s|}, \quad \tilde{u}_0(s) = \begin{pmatrix} 0 \\ \Gamma \text{sign}(s) \\ \epsilon \end{pmatrix}$$

and

$$\check{w}_{odd} = \frac{\tilde{C} \text{sign}(s)}{\sqrt{\Gamma^2 - \epsilon^2}} \check{u}_-(s) \quad (76)$$

Equation (74a) gives

$$\tilde{C} = \frac{\sin \delta\alpha (\Gamma - C\epsilon)}{\sqrt{\Gamma^2 - \epsilon^2} \cos \delta\alpha - \Gamma} \quad (77)$$

Using Eqs. (41), (76), and (77) we find the combinations  $\zeta(s_0) \pm \zeta(-s_0)$ ,  $\theta(s_0) \pm \theta(-s_0)$ , and  $ig(s_0) + ig(-s_0)$  in terms of the coefficient  $C$ . Next we insert these combinations into Eq. (74b) and find

$$C[\epsilon - 2ZI_{odd}] = \Gamma + 2\epsilon I_{odd} \cos \delta\alpha \quad (78)$$

where

$$Z = \frac{[\sqrt{\Gamma^2 - \epsilon^2} \cos \delta\alpha - \Gamma]^2 - \epsilon^2 \sin^2 \delta\alpha}{\sqrt{\Gamma^2 - \epsilon^2} - \Gamma \cos \delta\alpha} \quad (79)$$

Equations (78), (79) are the counterparts of Eq. (46) for an asymmetric case and transform into it for  $\delta\alpha \rightarrow 0$ .

For  $\epsilon \ll \Gamma$  we have  $Z = 1 - \cos \delta\alpha$ . For  $\delta\alpha \gtrsim \epsilon/\Delta$  the integral  $I_{odd}$  Eq. (75) has only imaginary part. Therefore,

$$C = \frac{\Gamma}{\epsilon - \epsilon_2(b) \pm i\gamma} \quad (80)$$

where

$$\gamma = \frac{\pi v_{\parallel} \Gamma \tan(\delta\alpha/2)}{\Lambda v_{2F} \Omega} e^{-K(\rho_0)} \sim \Gamma^2/\Delta, \quad (81)$$

and  $\rho_0 = |b/\sin \delta\alpha|$ . In Eq. (80) we include the energy  $\epsilon_2(b)$  which can be obtained by more detailed calculations taking into account corrections due to  $b/\rho$  in the same way as in Section IV. The function  $K(\rho_0)$  decays exponentially as  $e^{-\rho_0/\xi_S}$  for impact parameters larger than the primary core size,  $b \gtrsim \xi_S$ .

Therefore, the imaginary term in (80) does not disappear unless  $\delta\alpha$  is very small. It results in smearing of the adiabatic energy level  $\epsilon_2(b) \ll \Gamma$  and in a Lorentzian behavior of the DOS due to tunneling into the primary vortex core states. We remind that this result is obtained within the quasiclassical approximation.

## VI. DISORDER EFFECTS.

### A. Multiple core. Clean limit with incoherent tunneling.

We study the disorder effects by introducing the momentum scattering first into the tunneling process as described by the incoherent tunneling model. Since the tunneling is considered as a perturbation one can assume a specular QP scattering at the interface on the bulk side

and, thus, use the results of the previous section for the Green functions. The self-energy potentials are now obtained by averaging the Green functions Eqs. (31) – (33) over the trajectory direction:  $\check{\Sigma}_T = i\Gamma \langle \check{g}_S \rangle$ . This averaging does not affect, of course, the induced gap function (25) outside the primary vortex core and, thus, the spectrum  $\epsilon_2$  survives the influence of the tunnel barrier disorder at least for  $b > \xi_S$ . On the contrary, the sub-gap branches localized within the primary vortex core are completely destroyed. Such dramatic consequence of the momentum scattering is caused by the averaging of electronic wave functions with different impact parameters and consequent loss of information about the CdGM states of the primary vortex. A natural consequence of the momentum scattering is the appearance of a finite broadening of energy levels for trajectories with small impact parameters  $b \lesssim \xi_S$ . Matching the solutions in the core and at large distances gives the expression for the coefficient  $C$  for  $b \lesssim \xi_S$  and  $|\epsilon| \ll \Gamma$ ,

$$C \left[ \epsilon - \epsilon_2(b) + \frac{2\sqrt{\Gamma^2 - \epsilon^2}}{\hbar v_{2F}} \int_0^\infty \Sigma_1 ds - \frac{2\Gamma}{\hbar v_{2F}} \times \int_0^\infty \Sigma_I^{loc} ds \right] = \left[ \Gamma - \frac{2\epsilon}{\hbar v_{2F}} \int_0^\infty \Sigma_I^{loc} ds \right] \quad (82)$$

Since  $|\Sigma_1| \sim |\Sigma_I^{loc}| \sim \Gamma$  the pole of the coefficient  $C$  is located at small energies  $\epsilon \lesssim \Gamma^2/\Delta \ll \Gamma$ . Thus, for  $\epsilon \ll \Gamma$  the expression for this coefficient takes the form

$$C \left[ \epsilon - \epsilon_2(b) + \frac{2}{\xi_{2D}} \int_0^\infty (\Sigma_1 - \Sigma_I^{loc}) ds \right] = \Gamma. \quad (83)$$

The localized self energies  $\Sigma_1$  and  $\Sigma_I^{loc}$  can be neglected for  $\epsilon \sim \Gamma$ . They also vanish for  $|b| \gg \xi_S$ . In both these limits, Eq. (82) transforms into Eq. (46). The integral term in the equation above can be written in terms of its real  $\beta(b) = \beta_I(b) - \beta_1(b)$  and imaginary  $\gamma(b) = \gamma_I(b) - \gamma_1(b)$  parts as follows:

$$\frac{2}{\xi_{2D}} \int_0^\infty (\Sigma_1 - \Sigma_I^{loc}) ds = -\beta(b) \pm i\gamma(b). \quad (84)$$

Here upper (lower) sign corresponds to the retarded (advanced) Green function. Further we calculate the terms of real  $\beta_{1,I}$  and imaginary  $\gamma_{1,I}$  parts of the integral (84), which are defined by the following expressions

$$\beta_\alpha(b) = \frac{2}{\xi_{2D}} \int_0^\infty \Re \Sigma_\alpha(s) ds, \quad \gamma_\alpha(b) = \frac{2}{\xi_{2D}} \int_0^\infty \Im \Sigma_\alpha(s) ds$$

and play the role of energy shifting and spectral branch broadening, respectively:

$$N_\epsilon(s, b) = \frac{\Gamma \gamma(b) e^{-|s|/\xi_{2D}}}{[\epsilon - \epsilon_2(b) - \beta(b)]^2 + \gamma^2(b)}, \quad (85)$$

Since parameters  $\beta, \gamma \sim \Gamma/\Delta$  and  $\epsilon_2(b)/\Gamma \ll 1$  are small for  $b \ll \xi_{2D}$  and  $|\epsilon| > \Gamma$ , the LDOS reaches its bulk value

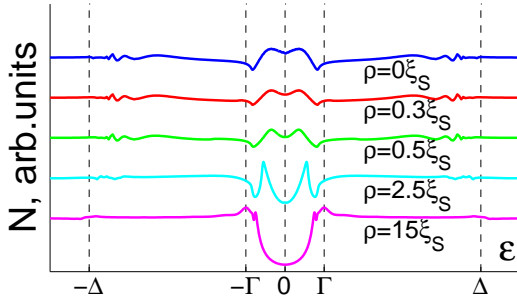


FIG. 8: (Color online) LDOS in logarithmic scale for incoherent tunneling in the clean limit. Curves, taken for different distances  $\rho$  from the vortex center, are vertically shifted for clarity. The peaks in LDOS exist up to distances  $\sim \xi_{2D}$ . Here  $\Delta/\Gamma = 5$ ,  $q_v = 1$ .

in this region:

$$N(\rho, \epsilon) = \frac{\sqrt{\epsilon^2 - \Gamma^2}}{|\epsilon|}. \quad (86)$$

Skipping the standard calculations of the above-defined integrals (84), we get the final expressions for parameters (see Appendix A for details):

$$\beta = \left\langle \frac{\Gamma^2 \pi q_v}{Q\Omega} \text{sign}(\epsilon + \Omega b) \right\rangle_z, \gamma = \left\langle \frac{\Gamma^2 q_v}{Q\Omega} \ln \frac{\Delta_\infty}{|\Omega b + \epsilon|} \right\rangle_z \quad (87)$$

The angular brackets denote averaging over the momentum  $Q_z$  along the vortex axis in bulk,  $\Omega = \partial\epsilon_0/\partial b$ . The DOS has a peak of height  $\Gamma/\gamma$  at an energy  $\epsilon = \epsilon_2(b) + \beta(b)$  shifted from the standard bound state level. This shift results in splitting of the ZBA<sup>32</sup> (Fig. 8). For calculations we use the numerical procedure similar to that used earlier for the coherent limit; the induced potentials were averaged over the cylindrical Fermi surface in the bulk.

### B. Multiple core. Dirty SC with clean 2D layer.

Smearing of the energy dependence of the induced potentials caused by disorder becomes even stronger if the bulk SC has a short mean free path:  $\ell \ll \xi_S$ . In dirty limit, the momentum averaged retarded (advanced) Green functions are parameterized as follows:

$$\check{g}_S^{R(A)}(\rho) = \check{\tau}_3 \sin \Theta^{R(A)} + \check{\tau}_2 \cos \Theta^{R(A)} e^{-i\check{\tau}_3 \phi}. \quad (88)$$

We put  $\Theta^{R(A)} = \pm\Theta_1 + i\Theta_2$ . The boundary conditions for  $\rho \rightarrow 0$  are  $g^{R(A)} \rightarrow \pm 1$ ,  $f^{R(A)}, f^{\dagger R(A)} \rightarrow 0$  which requires  $\Theta_1 \rightarrow \pi/2$ ,  $\Theta_2 \rightarrow 0$ . At large distances  $\Theta_1 \rightarrow 0$ ,  $\tanh \Theta_2 \rightarrow -\epsilon/\Delta_\infty$  for  $\epsilon < \Delta_\infty$  while  $\Theta_1 \rightarrow \pi/2$ ,  $\tanh \Theta_2 \rightarrow -\Delta_\infty/\epsilon$  for  $\epsilon > \Delta_\infty$ . Then,  $\Theta_2 = 0$  for  $\epsilon \ll \Delta_\infty$ , and the Usadel equation becomes<sup>33</sup>

$$D_S \left[ \nabla^2 \Theta_1 + \frac{\sin(2\Theta_1)}{2\rho^2} \right] - 2\Delta_0 \sin \Theta_1 = 0. \quad (89)$$

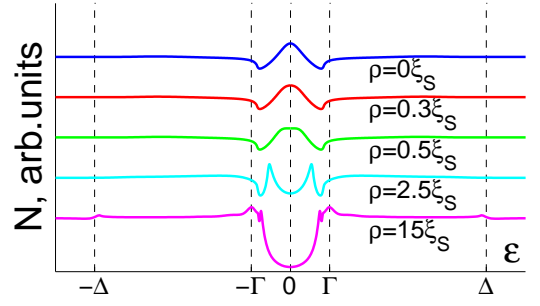


FIG. 9: (Color online) The local DOS in logarithmic scale for the dirty limit with the parameters  $\Delta/\Gamma = 5$ ,  $v_{2F}/V_F = 1$ . Curves, taken for different distances  $\rho$  from the vortex center, are vertically shifted for clarity.

The solution of Eq. (89) has been found in Ref. 33:  $\Theta_1(\rho)$  monotonously decays from  $\pi/2$  at the origin down to zero at  $\rho \gg \xi_S$ . The Green functions (88) determine the induced vortex potentials  $\check{\Sigma}_T = i\Gamma\check{g}_S$ .

For small impact parameter values  $b \ll \xi_S$  we get  $\Sigma_I^{loc} = 0$  and the matching condition takes the form:

$$\xi_{2D}\theta(s_0) = 2i\zeta(s_0) \int_0^\infty \sin \Theta ds + 2ig(s_0)b \ln[s_0/\xi_S]. \quad (90)$$

The coefficient  $C$  in this case has the only broadened pole at  $\epsilon = \epsilon_2(b)$ :

$$C[\epsilon - \epsilon_2(b) + i\gamma] = \Gamma, \quad (91)$$

where the broadening

$$\gamma = \frac{2\Gamma\sqrt{\Gamma^2 - \epsilon^2}}{\hbar v_{2F}} \int_0^\infty \sin \Theta ds,$$

where the integral is taken along the trajectory. For  $|\epsilon| < \Gamma$  and  $\rho < \xi_S$  the angle-resolved DOS can be written in the form

$$N_\epsilon(s, b) = \frac{\Gamma^2}{\sqrt{\Gamma^2 - \epsilon^2}} \frac{\gamma(b)e^{-\lambda|s|}}{[\epsilon - \epsilon_2(b)]^2 + \gamma^2(b)}. \quad (92)$$

Consequently, the LDOS has a peak of the height  $\sim \Gamma/\gamma(\rho)$  at energy  $\epsilon = \epsilon_2(\rho)$ .

For the energies above the induced gap  $\epsilon > \Gamma$  and small impact parameter values  $\epsilon_2(b), \gamma(b) \ll \Gamma$  the local DOS can be replaced by its bulk value:

$$N(\rho, \epsilon) = \frac{\sqrt{\epsilon^2 - \Gamma^2}}{|\epsilon|} \quad (93)$$

For  $b \gg \xi_S$  the imaginary part of energy decays exponentially, and Eq. (91) transforms into Eq. (46).

The numerical results shown in Fig. 9 clearly demonstrate the broad peak in the LDOS; this peak shifts and becomes sharper as the distance from the vortex center increases. For  $\rho \gg \xi_S$ , the LDOS approaches that obtained for the clean limit in Figs 6 and 8. For calculations we used the standard relaxation method<sup>34</sup> of solving the Usadel equation in the bulk and the Riccati parametrization for Eilenberger equations in the 2D layer.

### C. Vortex core expansion. Dirty SC and 2D layer.

To complete our analysis we briefly discuss the case of strong disorder both in the bulk SC and in the 2D layer. In this limit our model reduces to the one studied numerically in Ref. 35. The condition  $\xi_S \ll \xi_{2D} = \sqrt{\hbar D_{2D}/\Gamma}$  ensures that the short-distance inhomogeneity in the induced vortex potentials inside the primary core region does not disturb the adiabatic solution based on Eq. (25). Indeed, for momentum-orientation-averaged Green functions in 2D layer

$$\check{g}(\rho) = \begin{pmatrix} g_2 & f_2 e^{i\phi} \\ -f_2^\dagger e^{-i\phi} & \bar{g}_2 \end{pmatrix} = \int \frac{d^2 k}{(2\pi)^2} \check{g}(\mathbf{k}, \mathbf{r})$$

one can derive the equation:

$$iD_{2D} [g_2(\nabla^2 - \rho^{-2})f_2 - f_2\nabla^2 g_2] - 2(\epsilon + \Sigma_1)f_2 + 2\tilde{\Sigma}_2 g_2 = 0, \quad (94)$$

with  $\tilde{\Sigma}_2 = \Sigma_2 e^{-i\phi}$ . This equation is similar to that derived by Kupriyanov<sup>36</sup> for a contact of two dirty superconductors.

Using a standard parametrization  $\check{g}(\rho) = \tau_3 \sin \Psi + \tau_2 \cos \Psi e^{-i\tau_3 \phi}$  and the expressions for the vortex potentials one can obtain the following equation

$$iD_{2D} \left[ \nabla_\rho^2 \Psi - \frac{\sin 2\Psi}{2\rho^2} \right] - 2\Gamma \sin(\Psi - \Theta) - 2i\epsilon \cos \Psi = 0, \quad (95)$$

where  $\nabla^2 = \rho^{-1} \partial_\rho (\rho \partial_\rho)$  and  $D_{2D} = \hbar v_{2F}^2 \tau / 2 - 2D$  diffusion coefficient. Integrating Eq. (95), multiplied by  $\rho$ , in a small region around the origin (from  $\rho = 0$  to the value  $\xi_S \ll \rho_0 \ll \xi_{2D}$ ) we find the matching condition for the adiabatic Green function (41, 42):

$$D_{2D} \left[ \rho \frac{\partial}{\partial \rho} \Psi \Big|_0^{\rho_0} + \int_0^{\rho_0} \frac{\sin 2\Psi}{2\rho} d\rho \right] - 2 \int_0^{\rho_0} \rho d\rho [\Gamma \sin(\Psi - \Theta) + i\epsilon \cos \Psi] = 0. \quad (96)$$

Considering the expansion  $\Psi(\rho_0) = \Psi_0 - K\rho_0$  with  $K = \partial\Psi(\rho_0)/\partial\rho \sim \xi_{2D}^{-1}$  and assuming  $\Psi_0 \neq \pi/2$  one obtains  $\cos \Psi_0 \approx \rho_0^2 / (\xi_{2D}^2 \ln(\rho_0/\xi_S)) \ll 1$ . This estimate confirms the conclusion that the LDOS in the dirty limit follows the bulk LDOS pattern scaled with the 2D coherence length  $\xi_{2D}$  to within the second order terms in the small parameter  $\rho_0/\xi_{2D}$ .

The resulting problem at low energies  $\epsilon \ll \Delta_\infty$  coincides with that describing a standard vortex in a dirty SC<sup>37</sup> with the gap value  $\Gamma$ . Thus, the full disordered system should reveal the same LDOS patterns as in the bulk case, though scaled with the much larger coherence length  $\xi_{2D}$  instead of  $\xi_S$ . This vortex-core expansion can account for anomalously large vortex images observed in  $MgB_2$ <sup>38</sup> and in high- $T_c$  cuprates<sup>39</sup>.

### VII. DISCUSSION.

The results described above imply that the electronic states in the induced superconducting configurations strongly depend on the tunneling mechanism and on the crystal structure of bulk and 2D materials. The structure and symmetry of electronic states can be essentially different from those in the bulk SC. This imposes severe restrictions on possible realization of various exotic proximity electronic states<sup>26,27</sup> including Majorana states<sup>9</sup> and, in particular, Majorana states in the vortex cores. Our results directly show that the existence of zero-energy states in the proximity induced vortex core crucially depends on the tunneling mechanism underlying the proximity coupling between the 2D layer and bulk SC. One expects that the zero energy core state can exist for coherent tunneling between SC and 2D layer both having isotropic Fermi surfaces, provided the symmetry of the induced superconducting order permits.

It is known that a zero energy core state exists for a vortex with an odd vorticity in graphene monolayer with intrinsic superconductivity<sup>41-43</sup>. The graphene monolayer with proximity-induced superconductivity thus would seem to be a good candidate to look for a zero energy state. However, the Fermi surface of graphene is highly anisotropic; it lies near the Dirac corners of the Brillouin zone with the group velocity directed radially from the Dirac points. This group velocity direction does not coincide with the direction of the Fermi momentum and of the Fermi velocity in the bulk SC as shown in Fig. 7. Though the results of the previous sections were obtained within the quasiclassical approximation, they still can shed a light on the possibility of the zero energy state in graphene, especially for sufficient doping level when the quasiclassical approximation for graphene is justified<sup>43</sup>. In this case the results of Sec.VB can be applied. They show that each state in the induced vortex core with energy  $\epsilon$  is coupled to an infinite set of levels in the primary core. It is the integral  $I_{odd}$  which accounts for these states. Its real part deals with off-resonance states with eigen-energies not equal to  $\epsilon$ , while the imaginary part comes from the resonance state with the same eigen-energy  $\epsilon$ . According to Sec.VB, the real part of the integral  $I_{odd}$  disappears for  $\epsilon = 0$  and  $b = 0$ . The fate of the imaginary part depends on that is the zero energy in resonance with any state in the primary core or not. It is known that for an s-wave clean bulk superconductor the core levels are discrete with a minigap  $\omega_0 \sim \Delta^2/E_F$  and no one lies at zero energy. Therefore, if the levels in the bulk are not broadened by disorder or by inelastic scattering, the imaginary part of  $I_{odd}$  does not appear, and the zero-energy state seems to be intact. The discrete nature of the core states is, of course, beyond the quasiclassical approximation. Therefore, the above consideration gives only a hint towards the possibility of zero energy state. The detailed analysis is needed which would be based on the strict quantum mechanical description. Note that an alternative possibility to save the zero energy states in-

roducing a cylindrical cavity in the bulk superconductor has been considered in Refs.<sup>21,22</sup>.

Other important feature of induced superconductivity in a LD system is an extremely large coherence length  $\xi_{2D}$ . It provides a unique possibility to realize vortex configurations with quite unusual parameters. Here we discuss briefly some configurations which are of interest. The detailed analysis of all these situations requires special considerations which we postpone to future work. First of all we note that the results of Sections III, V and the following sections are valid for  $\xi_{2D} \ll \min(r_v, \lambda_L)$  where  $r_v$  is the intervortex distance and  $\lambda_L$  is the London penetration length in bulk SC. If the vortex lattice in the bulk SC is dense enough with the intervortex distance  $\xi_{2D} \lesssim r_v \ll \lambda_L$ , the induced 2D vortex cores may start to overlap. The spectrum  $\epsilon_2$  will then be modified due to intervortex tunneling of QPs (see Ref.<sup>44</sup>). The effect of the intervortex QP tunneling should be important provided the splitting of the quantized energy levels due to this tunneling exceeds the minigap value. The splitting can be estimated as  $\Gamma \exp[-r_v/\xi_{2D}]$  while the minigap inside the induced vortex core is of the order of  $\Gamma^2/\hbar v_{2F} k_{2F}$ . Thus, the ratio determining the intervortex tunneling efficiency is the exponent with a big prefactor,  $\hbar v_{2F} k_{2F} \Gamma^{-1} \exp[-r_v/\xi_{2D}]$ . It is this ratio which controls the interplay between the velocity of the trajectory precession and QP tunneling speed. The changes in the QP spectrum become essential when  $r_v \lesssim \xi_{2D} \ln(\hbar v_{2F} k_{2F}/\Gamma)$ . The minigap in this case should vanish according to the analysis in Ref. 44.

In some cases the 2D coherence length  $\xi_{2D}$  can exceed the London penetration depth  $\lambda_L$ ; this depends on the properties of bulk SC and on the tunneling rate  $\Gamma$ . If  $\xi_{2D}, r_v \gg \lambda_L$  the superconducting velocity vanishes along the trajectories with  $b > \lambda_L$ , thus the spectral branch  $\epsilon_2(b)$  saturates already for  $b \sim \lambda_L$ .

Our results for coherent tunneling can be directly generalized for clean  $d$ -wave bulk SCs with isotropic Fermi surfaces. However, the incoherent tunneling destroys the superconducting coherence in the 2D layer. As a result, the branch  $\epsilon_2$  disappears, while the QP states for  $\epsilon < \Delta$  have finite lifetimes for distances close to the vortex cores in bulk SC.

Considering possible experimental realizations of the induced vortex states one has to remember of the finite dimensions  $L$  of the 2D layer. The large size of the induced vortex cores can lead to the situation typical for mesoscopic superconducting samples when  $L$  is close to several  $\xi_{2D}$ 's. The criterion when the vortex spectrum transformation caused by the boundary effects in such systems becomes important can be found using the results of Ref. 40. One only needs to replace the gap, the coherence length and the minigap by the appropriate values in the 2D layer. The criterion appears to be very similar to that describing the efficiency of intervortex tunneling: the mesoscopic fluctuations of quantum levels in the 2D core become comparable with the minigap for  $L \lesssim \xi_{2D} \ln(\hbar v_{2F} k_{2F}/\Gamma)$ .

In conclusion, the model of proximity coupled 2D layer gives the possibility to study theoretically many spatially inhomogeneous situations including various configurations of induced vortices. Based on this model we have presented here description of the vortex core states for some typical tunneling mechanisms. In particular, our results can be used for interpreting the STM data on the vortex LDOS in superconductors through the model of a thin proximity layer present at the surface of the bulk SC. Effect of a thin non-superconducting proximity layer can explain various experimentally observed features of the vortex LDOS and reveals that STM technique alone is not sufficient for identifying multicomponent or anisotropic energy gap.

### Acknowledgments

We thank A. Buzdin, G. Volovik and A. Smirnov for stimulating discussions. This work was supported in part by EU 7th Framework Programme (FP7/2007-2013, Grant No. 228464 Microkelvin) and by the Academy of Finland through its LTQ CoE grant (project no. 250280), by the Russian Foundation for Basic Research, by the Program ‘‘Quantum Physics of Condensed Matter’’ of the Russian Academy of Sciences, the Russian president foundation (SP- 1491.2012.5), and by FTP ‘‘Scientific and educational personnel of innovative Russia in 2009-2013’’.

### Appendix A: Calculation of self energies for incoherent tunneling

Assuming small impact parameter values  $b \ll \xi_S$ , i.e., we calculate in this Appendix the following integrals from the main text:

$$\beta_\alpha(b) = \frac{2}{\xi_{2D}} \int_0^\infty \Re \Sigma_\alpha(s) ds, \quad \gamma_\alpha(b) = \frac{2}{\xi_{2D}} \int_0^\infty \Im \Sigma_\alpha(s) ds.$$

For this purpose we consider the case of the small impact parameter values  $b \ll \xi_S$ :

$$\beta_I(b) = \frac{2\Gamma^2 b}{v_{2F}} \int_0^\infty \left\langle \frac{v_{\parallel} e^{-K}}{2Q\Omega\rho^2} \times \left[ 1 - \Re \frac{|e|}{\sqrt{\epsilon^2 - \Omega^2 \rho^2}} \right] \right\rangle_z ds,$$

where  $\rho^2 = b^2 + s^2$ . In this case the first term in the above integral is determined by  $s \sim b$ :

$$\begin{aligned} \Gamma b \int_0^\infty \left\langle \frac{v_{\parallel} e^{-K}}{Q\Omega\rho^2} \right\rangle_z ds &= \Gamma b \int_0^\infty \left\langle \frac{v_{\parallel}}{Q\Omega(s^2 + b^2)} \right\rangle_z ds \\ &= \text{sign}(b) \Gamma \left\langle \frac{\pi v_{\parallel}}{2Q\Omega} \right\rangle_z. \end{aligned}$$

The second one is determined by very small impact parameters and reads:

$$\int_0^{b_0} \frac{ds}{\sqrt{b_0^2 - s^2}} = \frac{\pi}{2}, \quad \int_0^{b_0} \frac{ds}{(s^2 + b_0^2)\sqrt{b_0^2 - s^2}} = \frac{\pi\Omega}{2|b\epsilon|},$$

where  $b_0^2 = \epsilon^2/\Omega^2 - b^2 > 0$ . As a result, we find:

$$\beta_I(b) = \text{sign}(b) \frac{\Gamma^2}{v_{2F}} \left\langle \frac{\pi v_{\parallel}}{Q\Omega} \chi(\Omega^2 b^2 - \epsilon^2) \right\rangle_z,$$

$$\beta_1(b) = -\text{sign}(\epsilon) \frac{\Gamma^2}{v_{2F}} \left\langle \frac{\pi v_{\parallel}}{Q\Omega} \chi(\epsilon^2 - \Omega^2 b^2) \right\rangle_z.$$

Here  $\chi(x)$  is the Heaviside theta-function, i.e.,  $\chi(x) = 1$  for  $x > 0$  and  $\chi(x) = 0$  for  $x < 0$ .

After simplifying the expression for  $\beta(b) = \beta_I(b) - \beta_1(b)$  we obtain (87). For  $b \gtrsim \xi_S$  the quantity  $\beta(b)$  decays as  $\exp(-2b/\xi_S)$ .

The expressions for imaginary parts hold for any distances  $\rho$  because the delta functions in the integrals select only the trajectories that pass at small impact parameters:

$$\begin{aligned} \gamma_1(b) &= \frac{\Gamma^2}{v_{2F}} \int_0^{\infty} \left\langle \frac{v_{\parallel} e^{-K}}{Q\sqrt{\Omega^2 \rho^2 - \epsilon^2}} \chi(\Omega^2 \rho^2 - \epsilon^2) \right\rangle_z ds \\ &= \frac{\Gamma^2}{v_{2F}} \left\langle \frac{v_{\parallel}}{Q\Omega} \ln \frac{\Delta_{\infty}}{\sqrt{|\Omega^2 b^2 - \epsilon^2|}} \right\rangle_z, \end{aligned}$$

$$\begin{aligned} \gamma_I(b) &= \frac{\Gamma^2 b}{v_{2F}} \int_0^{\infty} \left\langle \frac{\epsilon}{\Omega \rho^2} \frac{v_{\parallel} e^{-K}}{Q\sqrt{\Omega^2 \rho^2 - \epsilon^2}} \chi(\Omega^2 \rho^2 - \epsilon^2) \right\rangle_z ds \\ &= \text{sign}(b\epsilon) \frac{\Gamma^2}{v_{2F}} \left\langle \frac{v_{\parallel}}{Q\Omega} \ln \frac{\Omega|b| + |\epsilon|}{\sqrt{|\Omega^2 b^2 - \epsilon^2|}} \right\rangle_z. \end{aligned}$$

Here we use the following expressions for the standard integrals:

$$\int_{b_0}^{s_{max}} \frac{ds}{\sqrt{s^2 \pm b_0^2}} = \ln \frac{\Delta}{\sqrt{|\Omega^2 b^2 - \epsilon^2|}},$$

where  $s_{max} \sim \xi_S$ , and

$$\int_{b_0}^{s_{max}} \frac{ds}{\sqrt{s^2 \pm b_0^2}(s^2 + b^2)} = \frac{\Omega}{|b\epsilon|} \ln \frac{\Omega|b| + |\epsilon|}{\sqrt{|\Omega^2 b^2 - \epsilon^2|}}.$$

The imaginary terms also decay exponentially for  $b \gtrsim \xi_S$ . The expression for  $\gamma(b) = \gamma_1(b) - \gamma_I(b)$  gives (87).

- 
- <sup>1</sup> W. L. McMillan Phys. Rev. **175**, 537 (1968).  
<sup>2</sup> P. G. de Gennes, *Superconductivity of Metals and Alloys* (Addison-Wesley, New York, 1989).  
<sup>3</sup> C. W. J. Beenakker Rev. Mod. Phys. **80**, 1337, (2008).  
<sup>4</sup> A. H. Castro Neto, F. Guinea, N.M. Peres, K.S. Novoselov, and A.K. Geim, Rev. Mod. Phys. **81**, 109 (2009).  
<sup>5</sup> M. Kociak, A. Yu. Kasumov, S. Guéron, B. Reulet, I. I. Khodos, Yu. B. Gorbatov, V. T. Volkov, L. Vaccarini, and H. Bouchiat, Phys. Rev. Lett. **86**, 2416 (2001).  
<sup>6</sup> J. C. Charlier, X. Blase, and S. Roche, Rev. Mod. Phys. **79**, 677 (2007).  
<sup>7</sup> Xiao-Liang Qi and Shou-Cheng Zhang, Rev. Mod. Phys. **83**, 1057 (2011).  
<sup>8</sup> H. B. Heersche, P. Jarillo-Herrero, J. B. Oostinga, L. M. K. Vandersypen, and A. F. Morpurgo, Solid State Commun. **143**, 72 (2007);  
<sup>9</sup> L. Fu, C. L. Kane Phys. Rev. Lett., **100**, 096407 (2008).  
<sup>10</sup> J. Alicea Rep. Prog. Phys. **75**, 076501 (2012).  
<sup>11</sup> H. F. Hess *et al.*, Phys. Rev. Lett. **62**, 214 (1989); H. F. Hess, R. B. Robinson, and J. V. Waszczak, Phys. Rev. Lett. **64**, 2711 (1990); I. Guillamon *et al.*, Phys. Rev. Lett. **101**, 166407 (2008).  
<sup>12</sup> C. Caroli, P. G. de Gennes, and J. Matricon, Phys. Lett. **9**, 307 (1964).  
<sup>13</sup> N.B. Kopnin, Phys. Rev. B **57**, 11775 (1998); A.S. Mel'nikov, Phys. Rev. Lett. **86**, 4108 (2001).  
<sup>14</sup> Øystein Fischer *et al.*, Rev. Mod. Phys. **79**, 353 (2007).  
<sup>15</sup> A.E. Koshelev and A. A. Golubov, Phys. Rev. Lett. **90**, 177002 (2003).  
<sup>16</sup> F. Giubileo *et al.*, Phys. Rev. Lett. **87**, 177008 (2001).  
<sup>17</sup> N.B. Kopnin and A.S. Melnikov, Phys. Rev. B **84**, 064524 (2011).  
<sup>18</sup> A.F. Volkov *et al.*, Physica C **242**, 261 (1995).  
<sup>19</sup> G. Fagas *et al.*, Phys. Rev. B **71**, 224510 (2005).  
<sup>20</sup> J.D. Sau *et al.*, Phys. Rev. B **82**, 094522 (2010).  
<sup>21</sup> A.L. Rakhmanov, A.V. Rozhkov, and Franco Nori, Phys. Rev. B **84**, 075141 (2011).  
<sup>22</sup> P.A. Ioselevich, P.M. Ostrovsky, and M.V. Feigelman, Phys. Rev. B **86**, 035441 (2012).  
<sup>23</sup> N.B. Kopnin, *Theory of Nonequilibrium Superconductivity* (Oxford 2001).  
<sup>24</sup> A. A. Abrikosov, L. P. Gor'kov, I. E. Dzyaloshinskiy, *Metody kvantovoj teorii polya v statisticheskoj fizike* (Fizmatgiz 1962).  
<sup>25</sup> C. W. J. Beenakker, Phys. Rev. Lett. **97**, 067007 (2006).  
<sup>26</sup> Y. Oreg, G. Refael, and F. von Oppen, Phys. Rev. Lett. **105**, 177002 (2010).  
<sup>27</sup> E. Perfetto, Phys. Rev. Lett. **110**, 087001 (2013).  
<sup>28</sup> L. Kramer and W. Pesch, Z. Phys. **269**, 59 (1974).  
<sup>29</sup> G. E. Volovik, Pis'ma Zh. Eksp. Teor. Fiz. **57**, 233 (1993) [JETP Lett. **57**, 244 (1993)]; *The Universe in a Helium Droplet* (Oxford University Press, 2003).

- <sup>30</sup> K. Shiozaki, T. Fukui, and S. Fujimoto, Phys. Rev. B **86**, 125405 (2012).
- <sup>31</sup> N. Schopohl and K. Maki, Phys. Rev. B **52**, 490 (1995).
- <sup>32</sup> I. Maggio-Aprile, Ch. Renner, A. Erb, E. Walker, and Ø. Fischer, Phys. Rev. Lett. **75**, 2754 (1995); B. W. Hoogenboom, Ch. Renner, B. Revaz, I. Maggio-Aprile, and Ø. Fischer, Physica C **332**, 440 (2000); S. H. Pan, E. W. Hudson, A. K. Gupta, K.-W. Ng, H. Eisaki, S. Uchida, and J. C. Davis, Phys. Rev. Lett. **85**, 1536 (2000).
- <sup>33</sup> L.P. Gor'kov and N.B. Kopnin, Zh. Eksp. Teor. Fiz. **65**, 396 (1973) [Sov. Phys. JETP, **38**, 195 (1974)].
- <sup>34</sup> A. Berman, and R. J. Plemmons, *Nonnegative Matrices in the Mathematical Sciences* (SIAM, 1994).
- <sup>35</sup> A.A. Golubov, Czechoslovak Journal of Physics **46**, 569 (1996).
- <sup>36</sup> M.Yu. Kupriyanov, Sverhprovodimost': Fizika, Khimia, Tekhnika **2**, 5 (1989).
- <sup>37</sup> A. A. Golubov and U. Hartmann, Phys. Rev. Lett. **72**, 3602 (1994).
- <sup>38</sup> M. R. Eskildsen, M. Kugler, S. Tanaka, J. Jun, S. M. Kazakov, J. Karpinski, and Ø. Fischer, Phys. Rev. Lett. **89**, 187003 (2002).
- <sup>39</sup> A. D. Beyer, M. S. Grinolds, M. L. Teague, S. Tajima and N.-C. Yeh, Europhys. Lett. **87**, 37005 (2009).
- <sup>40</sup> N.B.Kopnin, A.S.Melnikov, V.I.Pozdnyakova, D.A.Ryzhov, I.A.Shereshevskii, and V.M.Vinokur, Phys. Rev. Lett. **95**, 197002 (2005); A. S. Mel'nikov, D. A. Ryzhov, and M. A. Silaev, Phys. Rev. B **78**, 064513 (2008).
- <sup>41</sup> R. Jackiw and P. Rossi, Nucl. Phys. B **190**, 681 (1981).
- <sup>42</sup> D. L. Bergman and K. L. Hur, cond-mat/0806.0379 (2008).
- <sup>43</sup> I. M. Khaymovich, N. B. Kopnin, A. S. Mel'nikov, and I. A. Shereshevskii, Phys. Rev. B **79**, 224506 (2009).
- <sup>44</sup> A. S. Mel'nikov and M. A. Silaev, Pis'ma Zh. Eksp. Teor. Fiz. **83**, 675 (2006) [JETP Lett. **83**, 578 (2006)].